Wear

Computational Investigation of the Effect of Microstructure on the Abrasive Wear Resistance of Tungsten-Carbide Nickel Composite Coatings

--Manuscript Draft--

Manuscript Number:	
Article Type:	Full length article
Keywords:	Artificial neural networks (ANNs), Finite element modelling, Johnson-Cook model, Johnson-Holmquist model, Machine learning, Nickel, Metal matrix composite coating (MMC), Scratch test, Tungsten carbide, Wear
Corresponding Author:	Mohammad Parsazadeh, Ph.D. University of Alberta Edmonton, AB CANADA
First Author:	Mohammad Parsazadeh, Ph.D.
Order of Authors:	Mohammad Parsazadeh, Ph.D.
	Gary A Fisher, PhD
	André McDonald, PhD
	James Hogan, PhD
Abstract:	Sliding wear was simulated for tungsten carbide-nickel (WC-Ni) composites with different WC particle sizes and volume fractions under various normal forces. Johnson-Cook and Johnson-Holmquist models were employed to simulate the mechanical behaviour of the Ni and WC phases, respectively. Using high-powered parallel computing, a detailed parametric study was conducted to understand the effects of normal force, WC particle size, WC particle volume fraction, and their interaction on the worn volume and the material removal mechanisms in WC-Ni metal matrix composite coating materials. This allowed for investigation of the competition and transition between microploughing, microcutting, and microfatigue. The results revealed that the stress was distributed better in the composite coating with higher particle volume fraction and smaller particle size, which increased the ability of the composite coating to resist deformation and wear. It was also found that the material removal mechanism changed from microploughing to microcutting with an increase in particle volume fraction. The worn volume was calculated for different combinations of intrinsic (e.g., WC particle size and volume fraction) and external (e.g., normal force) parameters considered in this study. The data obtained was used to train a machine learning-based model using artificial neural networks. The trained model was further employed to predict the worn volume, and the results revealed that a mechanistic modelling approach can predict worn volume reasonably well.
Suggested Reviewers:	Richard Chromik, PhD Professor, McGill richard.chromik@mcgill.ca Professor in materials engineering
	Sanjay Sampath, PhD Stony Brook University ssampath@ms.cc.sunysb.edu Professor in material science
	Adrian Gerlich, PhD University of Waterloo agerlich@uwaterloo.ca Professor in Materials science.
	Fardad Azarmi, PhD Professor, North Dakota State University fardad.azarmi@ndsu.edu Professor in materials science
	Kantesh Balani, PhD

	Indian Institute of Technology Kanpur kbalani@iitk.ac.in Professor in materials science

UNIVERSITY OF ALBERTA

DEPARTMENT OF MECHANICAL ENGINEERING

5-08F Department of Mechanical Engineering
9211 - 116 Street NW
Edmonton, Alberta, Canada T6G 1H9
www.mece.engineering.ualberta.ca

October 22, 2020

Drs. A. Fischer, M. Papini
Co-Editors-in-Chief, Wear

Re: Manuscript Submission

Dear Drs. Fischer and Papini

We are pleased to submit a research paper entitled "Computational Investigation of the Effect of Microstructure on the Abrasive Wear Resistance of Tungsten-Carbide Nickel Composite Coatings". This manuscript highlights our most recent findings regarding abrasive wear resistance of Tungsten Carbide (WC)-based metal matric composite (MMC) coatings. To date, limited studies have focused on the effect of the external and intrinsic factors on the wear resistance of WC-Ni composites and overlays. In experiments, controlling the factors, particularly intrinsic factors, affecting the scratch resistance is difficult. A few studies have used numerical approaches to unravel the effects of reinforcing particles on the local scratch and the mechanisms involved in plastic deformation and material removal of composite coatings. Also, to the best knowledge of the authors, no 3-D numerical simulation has been conducted to evaluate the effect of WC reinforcing particles on scratch resistance in WC-Ni composites. No model has been developed to predict the scratch resistance of WC-Ni composite coatings. Thus, this paper aims to: (1) numerically analyze the effect of both external and intrinsic factors affecting the scratch resistance of WC-Ni composite coatings, and (2) develop a model to predict the scratch resistance of the composite under study using the a machine-learning based approach, Artificial Neural Network.

To accomplish this, a finite element (FE) model was developed to simulate the scratch resistance of WC-Ni composite coatings with consideration for relevant material and damage models needed for scratch simulation. The FE model was validated with an experimental study published earlier. The effects of WC particles size, volume fraction, and load on the scratch resistance of the composite coating were evaluated, and an ANNs model was developed to predict the scratch resistance of the composite coating, which could be employed to optimize the composite in terms of the material wear. It is worth-mentioning that this manuscript is the first public report that developed this machine-learning based model to predict the scratch resistance of WC-Ni composite coating.

If any additional material is needed, please contact me.

Thank you for your consideration.

Sincerely,

Mohammad Parsazadeh, Ph.D, M.Sc., B.Eng.
Postdoctoral Fellow
Department of Mechanical Engineering
University of Alberta

Highlights

- FE model was developed to analyze the wear loss of WC-Ni composite coating.
- The FE model was used to study the material removal mechanisms.
- Effects of intrinsic and external factors on the wear resistance were analyzed.
- A machine learning-based model, ANN, was developed to predict the worn volume.

Computational Investigation of the Effect of Microstructure on the Abrasive Wear Resistance of Tungsten-Carbide Nickel Composite Coatings

Mohammad Parsazadeh[a,*], Gary Fisher[b], André McDonald[a], James Hogan[a]

[a] *Department of Mechanical Engineering, University of Alberta, Edmonton, Alberta T6G 1H9, Canada*

[b] *InnoTech Alberta, Edmonton, Alberta, T6N 1E4, Canada*

Abstract

Sliding wear was simulated for tungsten carbide-nickel (WC-Ni) composites with different WC particle sizes and volume fractions under various normal forces. Johnson-Cook and Johnson-Holmquist models were employed to simulate the mechanical behaviour of the Ni and WC phases, respectively. Using high-powered parallel computing, a detailed parametric study was conducted to understand the effects of normal force, WC particle size, WC particle volume fraction, and their interaction on the worn volume and the material removal mechanisms in WC-Ni metal matrix composite coating materials. This allowed for investigation of the competition and transition between microploughing, microcutting, and microfatigue. The results revealed that the stress was distributed better in the composite coating with higher particle volume fraction and smaller particle size, which increased the ability of the composite coating to resist deformation and wear. It was also found that the material removal mechanism changed from microploughing to microcutting with an increase in particle volume fraction. The worn volume was calculated for different

[*] Corresponding author: Email address: parsazad@ualberta.ca (Mohammad Parsazadeh)

combinations of intrinsic (e.g., WC particle size and volume fraction) and external (e.g., normal force) parameters considered in this study. The data obtained was used to train a machine learning-based model using artificial neural networks. The trained model was further employed to predict the worn volume, and the results revealed that a mechanistic modelling approach can predict worn volume reasonably well.

Keywords: Artificial neural networks (ANNs), Finite element modelling, Johnson-Cook model, Johnson-Holmquist model, Machine learning, Nickel, Metal matrix composite coating (MMC), Scratch test, Tungsten carbide, Wear

1. Introduction

The development of advanced coating materials with increased longevity [1] is important in the petroleum [2], aerospace [3], mining [4], and manufacturing industries [5,6], where high temperatures [7], corrosion [2], and wear [8] are common. Among types of coating materials used in these applications (e.g., silicon carbide (SiC) [9], boron carbide (B_4C) [10], titanium carbide (TiC) [11]), tungsten carbide (WC)-based metal matric composite (MMC) coatings and overlays are suitable choices given their unique combination of hardness and fracture toughness [12]. In these applications, WC is commonly combined with Ni-based alloys to serve as a metallic binder to effectively resist against wear damage [12–14].

The main factors influencing the abrasive wear performance of metal matrix composite coatings and overlays can be categorized as intrinsic or external factors [15]. Intrinsic factors include mechanical properties of both reinforcing particles and the matrix and microstructure of the composite coating and overlay (e.g., volume fraction [12,16], size [16,17], shape, and size distribution of the reinforcing particles). External factors include the loading condition [18], the shape and size of the abrasive particles [19, 20], temperature [21], and sliding velocity [22]. In the literature, models have been developed to describe the wear performance of MMCs [10, 23, 24]. The simplest and most fundamental model that was derived from complex abrasive wear conditions is the one-cycle interaction of a single abrasive particle and material [17, 18, 25, 26]. Commonly, this interaction is evaluated in a controlled scratch test [27], which is an experiment used by many researchers to evaluate the mechanical and wear behaviour of different materials (e.g., polymers [28], ceramics [29], metals [30], metal-matrix composites [9, 29, 30], and coatings [31, 32]). In this type of experiment, the scratching deformation [34] is a consequence of a combination of failure processes: 1) microploughing [35], 2) microcutting [36], 3) microfatigue [37], and 4) microcracking [37]. The competition of these mechanisms is material-dependent [38] and manifests as measurements of penetration and residual scratch depth [38]. These can be induced by controlling the normal load, indenter shape, and scratch speed. This study aims to explore these mechanisms through physics-based modelling of a scratching action of a rigid indenter with a predefined radius over a WC-Ni composite surface.

Scratch test experiments allow for better understanding of the mechanisms of wear and the effect of the intrinsic and external factors on the wear performance [39]. For example, ploughing was found to be dominant in a study conducted by Varga, *et al*. [40] to evaluate the effects of load and temperature on scratch mechanisms of austenitic steel, a cast steel with a carbide network, and a Ni-based material with a carbide network. The adhesion and hardness of electrodeposited Ni coatings were improved by heat treatment in another study conducted by Ul-Hamid, *et al*. [41], and the surface mechanical properties of Ni were evaluated at different progressive loads. Microscratch test of Ni coatings revealed that cracking and decohesion of Ni coatings do not occur at the highest final loads (30 N) that were considered in their study. Also, the deformation mechanisms were evaluated at different scratch velocities in nanostructured Ni [42] and nanostructured Ni with bimodal grain size distributions [43] and were found to be different compared with conventional coarse grain counterparts due to the different strain rate sensitivity of these materials. The effects of different grades of WC reinforcing particles and volume fraction on the microstructure and material removal behavior of the WC-Ni composite, for example, were analyzed by Alzouma *et al*. [17]. It was found that the composite becomes more wear-resistant when the reinforcing volume fraction is increased, which results in protection and strengthening of the matrix. Plastic deformation of the metal matrix was also reduced [17]. The results from these previous studies will be important in the present investigation on the effects of microstructure, mechanical properties, and loading conditions on the scratch response of WC-Ni composites.

Studying the effect of microstructure on wear mechanisms is difficult to analyze experimentally since fully controlling the intrinsic and external factors is challenging. Numerical simulation is an alternative to evaluate the contribution of individual factors on scratch resistance separately [18]. For example, the effect of the attack angle and load on the wear performance of glass fibre reinforced polyester composites were evaluated in a numerical study by Mzali, *et al*. [44]. Consideration was given to the cohesive zone between the fibre and matrix. The results revealed the significant effect of attack angle on the transition of wear mechanisms during ploughing to result in composite damage. Also, the effects of the size and volume fraction of WC particles on scratch resistance in WC-Ni composites were evaluated in a two-dimensional numerical model by Hu, *et al*. [45]. They later expanded their initial study [45] to analyze the effect of other parameters on material removal, such as WC particle shape, distribution of reinforcement, and their interaction with their volume fraction [46]. Hu, *et al*. [46] concluded that the composite material might benefit from the increase in hardness at the expense of toughness by increasing the volume fraction of the reinforcing particles. Among the studies reviewed above, a few of them numerically evaluated the scratch resistance of the composites; however, no model has been developed to predict the scratch resistance of WC-Ni composite coatings, as is pursued here.

As an alternative modelling approach to finite element analysis, artificial neural networks (ANNs) have attracted increasing interest due to the high capability of modelling highly nonlinear and complex problems [47–51]. To predict wear rates using ANNs, one of the first efforts was conducted by Jones, *et al*. [47] based on a limited set of experimental data. ANNs were also employed to predict the tribological properties of Al7075-Al_2O_3 composites [48], epoxy composites [49], rice husk ash reinforce aluminum alloys [50], and also to predict wheel and rail wear rates [51]. The results of these studies revealed that ANNs could be an appropriate approach to predict the scratch resistance of composite materials, as is pursued here.

To date, limited studies have focused on the effect of the external and intrinsic factors on the wear resistance of WC-Ni composites and overlays. In experiments, controlling the factors, particularly intrinsic factors, affecting the scratch resistance is difficult. A few studies have used numerical approaches to unravel the effects of reinforcing particles on the local scratch and the mechanisms involved in plastic deformation and material removal of composite coatings. Also, to the best knowledge of the authors, no 3-D numerical simulation has been conducted to evaluate the effect of WC reinforcing particles on scratch resistance in WC-Ni composites. No model has been developed to predict the scratch resistance of WC-Ni composite coatings. Thus, this paper aims to: (1) numerically analyze the effect of both external and intrinsic factors affecting the scratch resistance of WC-Ni composite coatings, which could also be applied to reasonably thick overlays, and (2) develop a model to predict the scratch resistance of the composite under study using the

ANNs approach. To accomplish this, a finite element (FE) model was developed to simulate the scratch resistance of WC-Ni composite coatings with consideration for relevant material and damage models needed for scratch simulation in Section 2. In the same section, the FE model was validated with an experimental study conducted by Ul-Hamid, *et al*. [52]. The effects of WC particles size (d_p), volume fraction (ϕ), and load on the scratch resistance of the composite coating were evaluated in Section 3, and an ANNs model was developed to predict the scratch resistance of the composite coating, which could be employed to optimize the composite in terms of the material wear.

2. Model and Theory

2.1. Physical Model

To evaluate the effects of various tribological scratch parameters (load, volume fraction, and particle size), a 3D model for scratch test simulation was developed. The scratch particle geometry was modelled on sand sizes observed in the Albertan oil sands, where the size distribution of these sands shown in Fig. 1 (a) was obtained using ImageJ software. It was found that the diameter of the sand varies from $55\ \mu\text{m}$ to $505\ \mu\text{m}$, and more than $75\ \%$ of these sands have a diameter range between 55 and $205\ \mu\text{m}$, as shown in Fig. 1 (b). The average sand diameter and the standard deviation were found to be $140\ \mu\text{m}$ and $78\ \mu\text{m}$, respectively. This average sand diameter was chosen as the diameter of the spherical indenter used in simulating scratch testing resistance. To reduce the computation time, the geometry size was also considered to be $0.40\times0.25\times0.60\ \text{mm}^3$. This geometry size was chosen according to the criterion introduced by Bucaille, *et al*. [53] and Tabor [54]. In this criterion, the geometry thickness must be four times greater than the scratch depth, and also the geometry width must be ten times greater than the scratch width. With these points in mind, the width and depth of the geometry were estimated by considering the scratch depth and width obtained for Ni in the studies conducted by UI-Hamid, *et al*. [52] and Zhu, *et al*. [43].

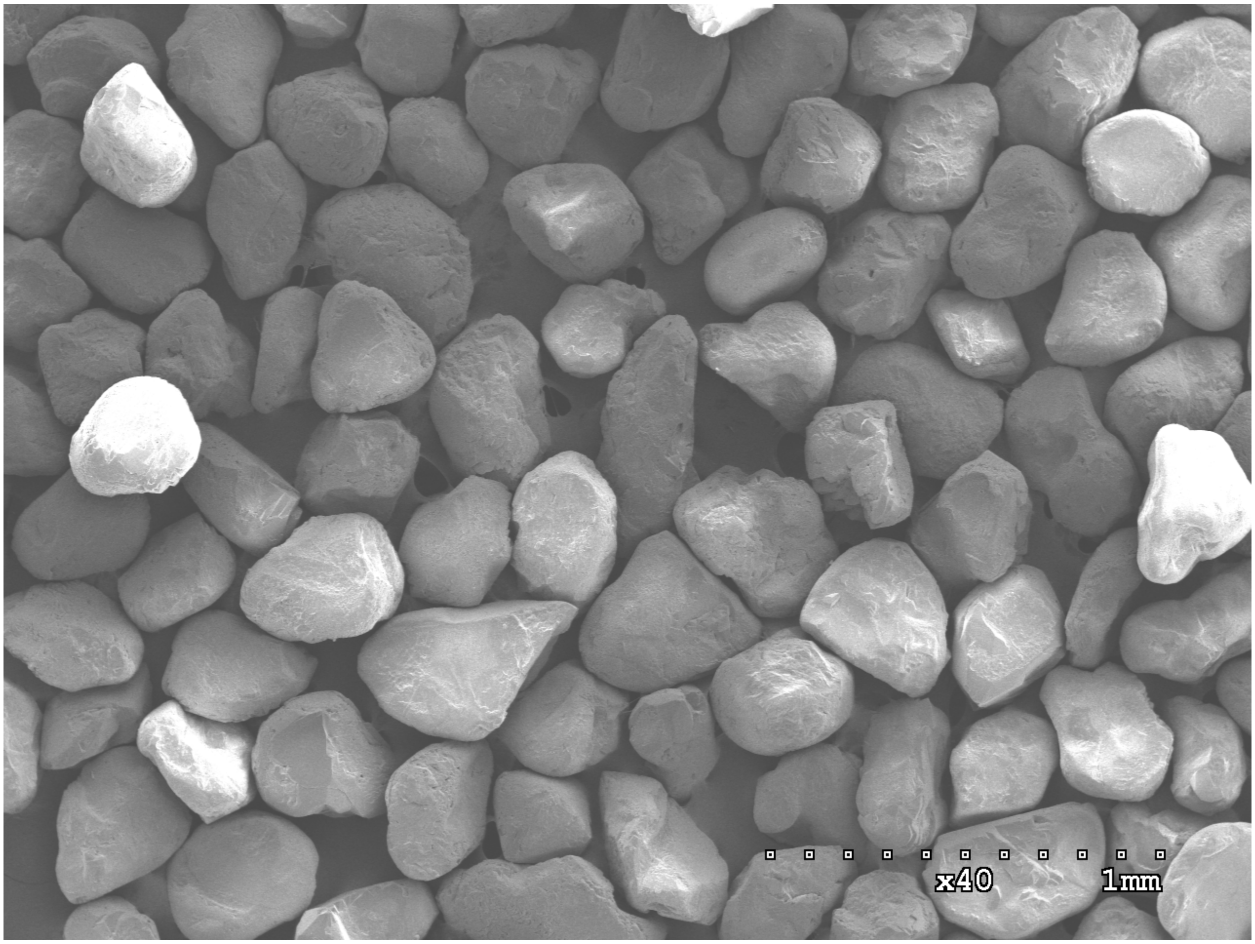

(a)

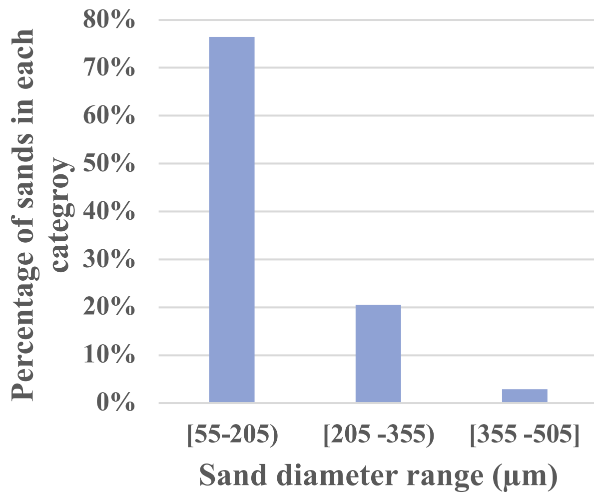

(b)

Fig. 1 (a) SEM images of different Alberta mine site sands (b) Sand size distribution.

The matrix and the reinforcing particles chosen in this study were considered as Ni and WC, respectively. This material was selected because of its unique combination of hardness and fracture toughness [12]. To evaluate the effect of the reinforcing particle size to the indenter size ratio on the material removal, three different WC particle diameters ($60\ \mu\text{m}$, $140\ \mu\text{m}$, and $220\ \mu\text{m}$) were chosen to have the size ratio smaller, equal, and larger than one. These different size ratios help better understand the different competing mechanisms that may affect material removal due to different reinforcing particle size to the indenter size. The volume fraction range of the WC particles was also considered to be $10-50$ Vol.%, with an increment of 20 Vol.%. The arrangement of the WC particles was also depicted for $\phi = 50$ Vol.% in Fig. 2 (a), and this range of reinforcing particles was motivated based on practical considerations and our applications of interest. A schematic diagram of the indenter and the composite coating is depicted in Fig. 2 (b). The bottom surface of the substrate was kept motionless, while an indenter carrying a certain load moved toward the *z*-direction.

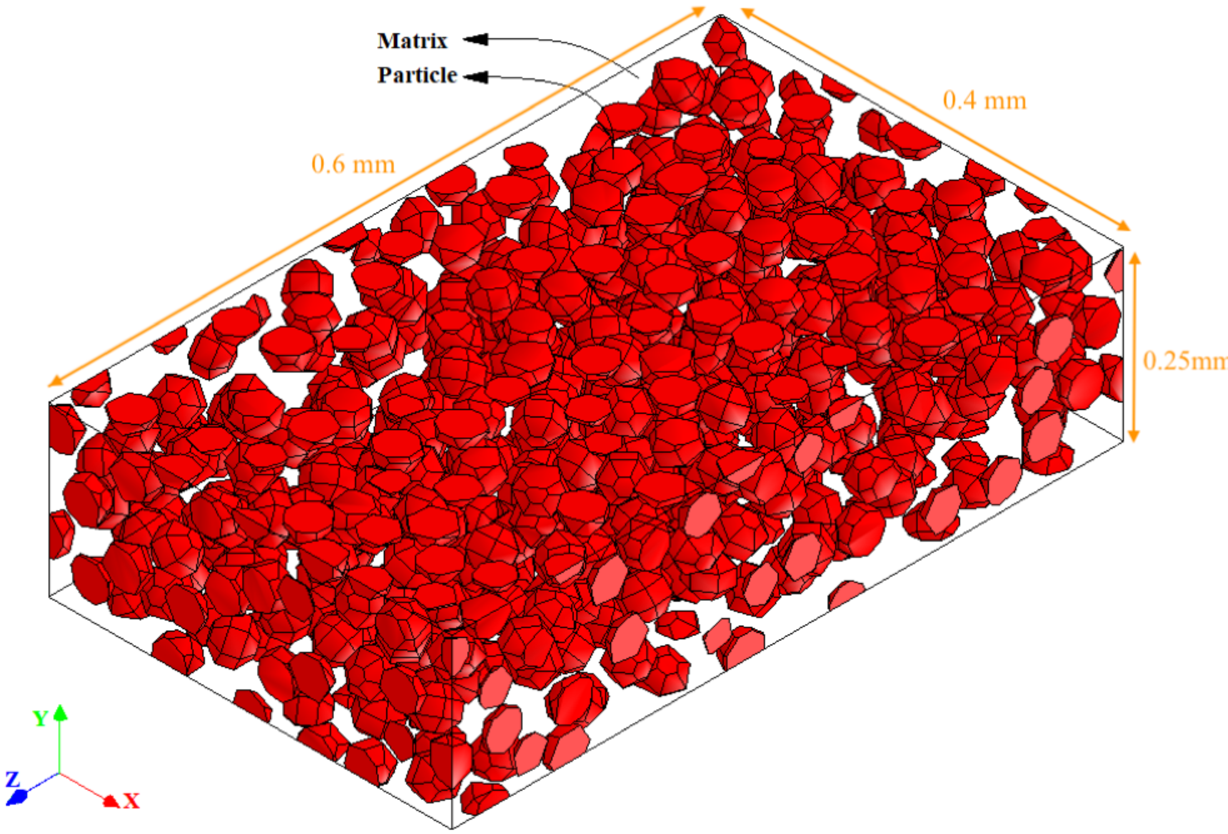

(a)

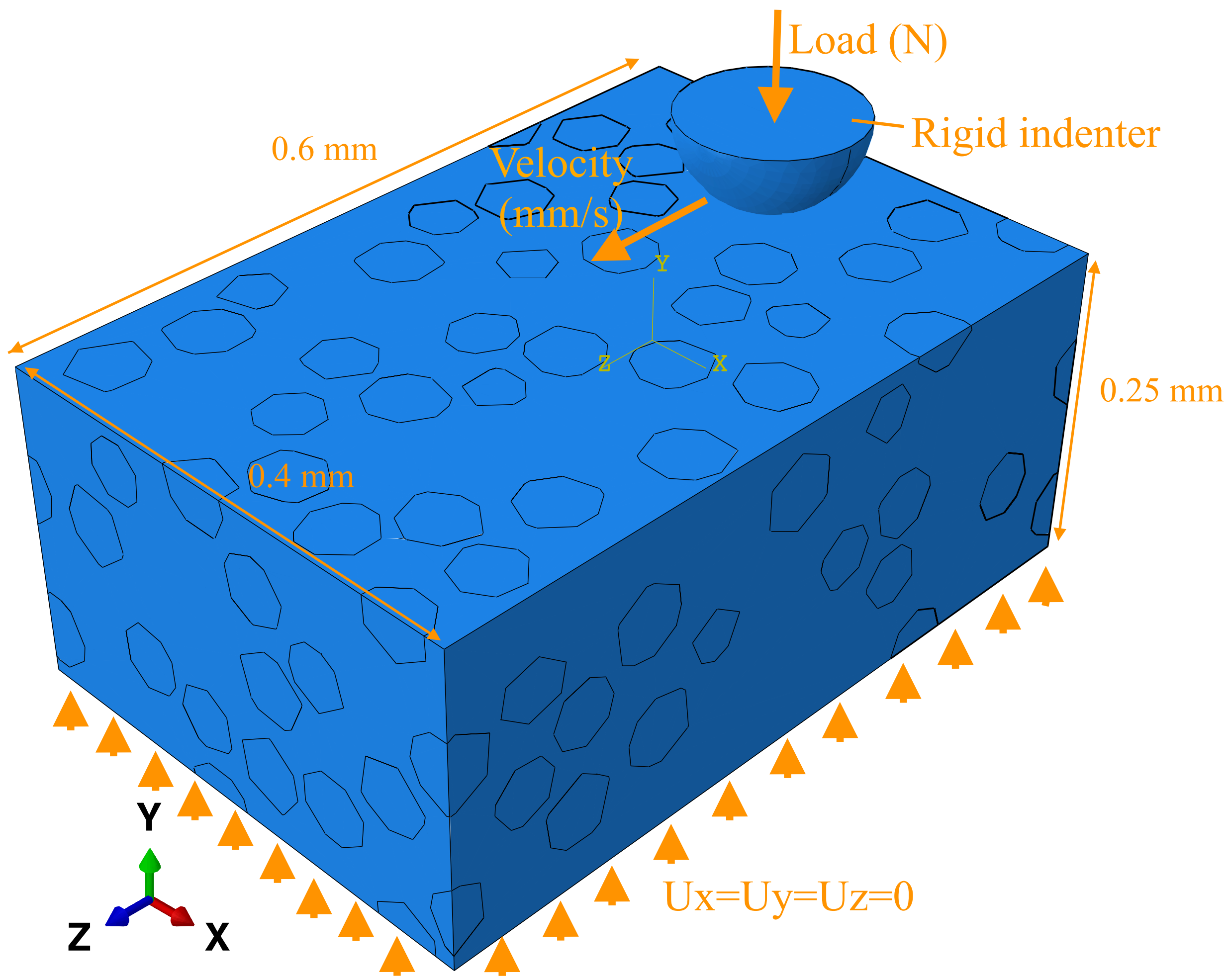

(b)

Fig. 2 The schematic diagram of (a) arrangement of the WC particles in the FE model ($\phi = 50$ Vol.%) (b) the indenter and the composite coating.

2.2. Finite Element Modelling

A finite element (FE) scratch model has been developed using Abaqus software. The model consists of a spherical rigid indenter and a flat deformable surface, as shown in Fig. 2 (b). The indenter was considered under a normal load varying between $1-9$ N pushing the indenter toward the substrate in the *y*-direction, and the indenter also moved in the *z*-direction with a constant velocity of 100 mm/s. The load range selected in this study will help understand the mechanisms affecting the material removal at small and large loads [18, 32, 54], and the indenter velocity was chosen large enough to avoid making the simulation computationally expensive. The substrate movement was constrained in all directions to evaluate the effect of the indenter over the substrate. The scratch simulation was completed under four steps. In the first step, surface-to-surface contact [18] was established between the indenter and the substrate, followed by increasing the normal load gradually until the load reached its maxima at the end of the second step. In the third step, the indenter moved with a constant velocity along the scratch length. During the last step, the indenter was unloaded and gradually lifted up by imposing a small magnitude of load in the opposite direction. The plastic deformation and material removal have been considered in the scratch model developed in this study using the Explicit option in Abaqus. The element types chosen to mesh the substrate and the indenter were a ten-node modified quadratic tetrahedron (C3D10M in ABAQUS FEA notation) and a 3-node 3-D rigid triangular facet (R3D3 in ABAQUS FEA notation), respectively. Compute Canada clusters were employed and paralleled to perform high-powered parallel computing, with typical run times of 15 hours on two nodes, each with 48 CPUs.

2.3. Constitutive Models

Two main approaches drawn from fracture mechanics [55, 56] and damage mechanics [57–59] were employed to model the material response under scratch loading. The matrix was modelled as an elastoplastic hardening material. To model the plasticity and damage behaviour of the Ni matrix under varying normal loads, the Johnson-Cook (J-C) constitutive equation [59] was employed.

In the J-C model, the relationship between von Mises flow stress (σ_{eq}), yield strength, hardening, and temperature softening is defined as:

$$\sigma_{eq} = \left[A + B(\bar{\varepsilon}^{pl})^N\right]\left[1 + C\ln\left(\frac{\dot{\bar{\varepsilon}}^{pl}}{\dot{\bar{\varepsilon}}_{\circ}^{pl}}\right)\right]\left[1 - \left(\frac{T - T_{ref}}{T_{melt} - T_{ref}}\right)^M\right], \tag{1}$$

where A is the yield strength, B is the strain-hardening modulus, $\bar{\varepsilon}^{pl}$ is the equivalent plastic strain, C is the strain rate hardening coefficient, $\dot{\bar{\varepsilon}}^{pl}$ is the equivalent plastic strain rate, $\dot{\bar{\varepsilon}}_{\circ}^{pl}$ is the reference strain rate, T is the temperature at operating condition, T_{ref} is the reference temperature, T_{melt} is the melting temperature, and N and M are strain the hardening exponent and softening exponent.

Based on the equivalent plastic strain ($\Delta\varepsilon^{pl}$), a damage parameter (D) was defined in the J-C damage model as:

$$D = \sum \frac{\Delta\varepsilon^{pl}}{\varepsilon_f^{pl}}, \tag{2}$$

where ε_f^{pl} is equivalent plastic strain at failure, which was defined as:

$$\varepsilon_f^{pl} = \left[D_1 + D_2 \exp\left(D_3\left(\frac{\sigma_m}{\sigma_{eq}}\right)\right)\right]\left[1 + D_4 \ln\left(\frac{\dot{\bar{\varepsilon}}^{pl}}{\dot{\bar{\varepsilon}}_{\circ}^{pl}}\right)\right]\left[1 + \frac{T - T_{ref}}{T_{melt} - T_{ref}}\right], \tag{3}$$

where D_1 to D_5 are material constants and σ_m is the mean stress.

In the J-C damage model, element removal occurs when the strain in the element exceeds the failure strain, which is when $D = 1$. At this stage, material stiffness decreases. This element removal leads to material loss on the surface that is under the sliding indenter. This modelling approach was also used in impact [59, 60] and erosion [61, 62] processes.

The Johnson-Holmquist (JH-2) constitutive model, which is based on the elastic-viscoplastic approach, was used to simulate the response of WC particles to deformation. This model is mainly used to simulate deformation in brittle materials (e.g., SiC [64], B_4C [65], and AlN [66]). In this model, the strength of the reinforcing particles is assumed to vary with changing pressure, strain rate, and tensile strength. Initially, elastic deformation is considered in the material. In this region, the stress-state is described based on the elastic material properties and equation of state. The relationship between pressure on the material and density ρ can be calculated based on the current material deformation as follows [66, 67]:

$$P = K_1\mu + K_2\mu^2 + K_3\mu^3 \quad if\, \mu \geq 0 \text{ and} \tag{4}$$

$$P = K_1\mu \quad if\, \mu \leq 0, \tag{5}$$

where $\mu = \rho / \rho_o$, ρ is the material density, ρ_o is a reference density, and K_1, K_2, and K_3 are constants (K_1 is the initial bulk modulus).

An increment in damage leads to material bulking, meaning that a larger volume is occupied by the fractured material compared with the intact condition. This leads to an increase in local pressure in a constrained material. Initially, the bulking pressure is zero for an undamaged material, and this bulking pressure can be calculated at the next time increment as [64, 65]:

$$\Delta P_{t+\Delta t} = -K_1\mu_{t+\Delta t} + \left[(K_1\mu_{t+\Delta t} + \Delta P_t)^2 + 2\beta K_1 \Delta U \right]^{1/2}, \tag{6}$$

where β is the fraction of elastic energy loss converted to potential hydrostatic energy and ΔU is energy loss due to increased bulking pressure, which is defined as [65–68]:

$$\Delta U = U(D) - U(D_{n+1}) \text{ and} \tag{7}$$

$$U(D) = \frac{\sigma}{6G}\ ,\tag{8}$$

where G is the elastic shear modulus.

In the JH-2 model, under compressive loading, the damage accumulates progressively with plastic deformation. A damage parameter, ranging from 0 to 1, is employed to track this damage accumulation, and this serves to degrade the overall strength in the material. The strength of the material is expressed in terms of the normalized von Mises equivalent stress as [66]:

$$\sigma^* = \sigma_i^* - D(\sigma_i^* - \sigma_f^*),\tag{9}$$

where D is the damage parameter, and σ_i^* and σ_f^* are the normalized intact and fractured equivalent stresses, respectively. These normalized equivalent stresses (σ^*, σ_i^*, and σ_f^*) have the general form of $\sigma^* = \sigma / \sigma_{HEL}$. In this definition, σ is the actual von Mises stress and σ^*_{HEL} is the equivalent stress at the Hugoniot elastic limit (HEL).

In the JH-2 model, the normalized intact and fractured stresses can be expressed as a function of pressure and strain rate as follows:

$$\sigma_i^* = A(P^* + T^*)^N (1 + C\ln\dot{\varepsilon}^*) \text{ and}\tag{10}$$

$$\sigma_f^* = B(P^*)^M (1 + C\ln\dot{\varepsilon}^*),\tag{11}$$

where A, B, C, M, and N are material constants, and P^* and T^* are the normalized pressure and normalized maximum tensile hydrostatic pressure, respectively, which can be defined as:

$$P^* = P / P_{HEL} \quad \text{and}\tag{12}$$

$$T^* = T / P_{HEL}, \quad (13)$$

where P_{HEL} is the pressure at the HEL and T is the maximum tensile pressure that a material can withstand.

To determine P_{HEL} and σ_{HEL}, HEL experimental data is required. HEL, which comprises of the pressure and deviatoric components, represents the point at which the shock wave exceeds the elastic limit of the material and is presented as a one-dimensional shock wave [66]. The HEL is defined by [65, 68]:

$$HEL = P_{HEL} + \frac{2}{3}\sigma_{HEL}. \quad (14)$$

Using Eq. (14), the value of P_{HEL} and σ_{HEL} were determined using the procedure described in several studies that implemented the JH-2 model [64, 65, 68]. The volumetric strain at HEL is determined using the following equation [66]:

$$HEL = K_1\mu_{HEL} + K_2\mu_{HEL}^2 + K_3\mu_{HEL}^3 + \frac{4}{3}G\frac{\mu_{HEL}}{1+\mu_{HEL}}. \quad (15)$$

The data presented in Moxnes, et al. [70] was employed to find the volumetric strain (μ_{HEL}) at HEL, and then this value was used in Eq. (4) to find P_{HEL}. Then, σ_{HEL} was determined using Eq. (14).

The damage evolution and fracture term of the model is similar to those in the J-C model described in Eq. (2). However, the fracture strain definition is different in this model and is given as:

$$\varepsilon_f^{pl} = D_1(P^* + T^*)^{D_2}, \quad (16)$$

where D_1 and D_2 are material constants.

All material parameters used in J-C and JH-2 models were listed in Table 1 along with other material properties and constants for Ni and WC. The Ni properties were obtained from Ghelichi, *et al*. [71], and WC properties were obtained from Moxnes, *et al*. [70] and Holmquist, *et al*. [72].

Table 1 Ni and WC properties and constants used in J-C and JH-2 constitutive models.

Material properties/parameters	Ni [71]	WC [69, 71]
A	163 [MPa]	0.9899
B	648 [MPa]	0.67
C	0.06	0
E	200 [GPa]	N/A
M	1.44	0.0322
N	0.33	0.0322
$\dot{\varepsilon}_{\circ}^{pl}$	1	1
ρ_o	8900 [kg/m^3]	14560 [kg/m^3]
υ	0.31	N/A
D_1	0.54	0.005
D_2	4.89	1
D_3	3.03	N/A
D_4	0.014	N/A
D_5	1.12	N/A

G	N/A	219 [GPa]
HEL	N/A	6.566 [GPa]
lDamage	N/A	0
K_1	N/A	362 [GPa]
K_2	N/A	694 [GPa]
K_3	N/A	0

2.4. Element Size and Model Validation

The FE model developed in this study needs to be independent of the number of elements and validated with experimental data. To perform validation, the results of this study were compared with the experimental study of Ul-Hamid, *et al*. [52] for the scratch testing of a low-porosity and fine-grained Ni material. This data set in this published study was the best validation case and aligned well with the low-porosity Nickel material that existed in our simulations. To reduce the computation time, the mesh independence test was conducted with increasing element size from 2,200 elements (element size of $60\ \mu m$) to 50,400 elements (element size of $5\ \mu m$). Choosing an optimum number of elements was important to reduce the computational time while keeping the results independent of the number of elements. The load on the indenter was considered to be 10 N, and the material undergoing the scratch was Ni with the material properties listed in Table 1. The average von Mises stress measured in the middle of the groove created by the scratch, and the scratch depth along the scratch length were calculated for different elements sizes and shown in Fig. 3. It was found that the average stress was independent of the element size when the number of elements was greater than 20,000 (element size of $10\ \mu m$), as shown in Fig. 3 (a). Similarly, the scratch depth did not significantly change when the number of elements was greater than 20,000, as depicted in Fig. 3(b). Thus, the minimum of 20,000 elements was chosen in this study to keep the results independent of the number of elements, while promoting computational efficiencies.

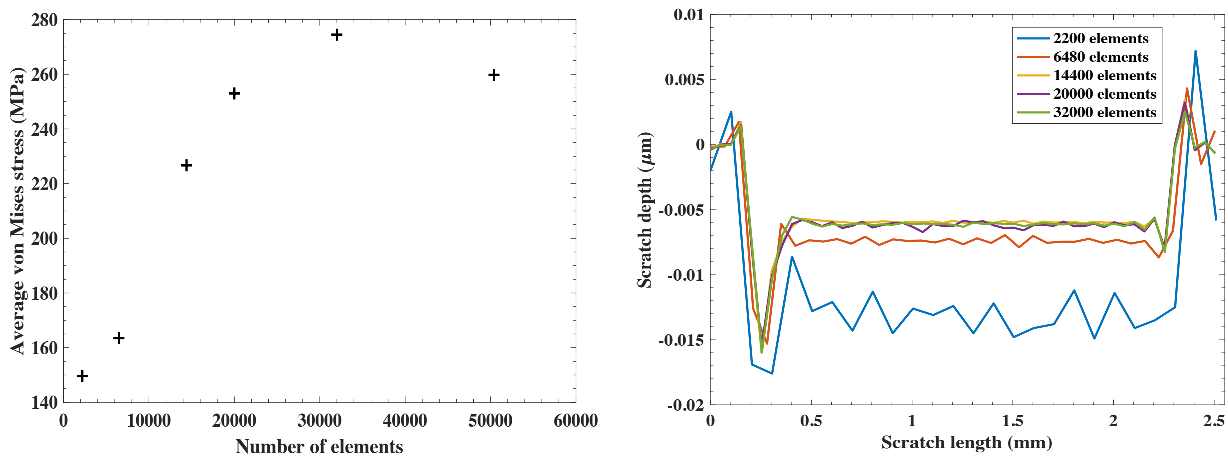

(a) (b)

Fig. 3 Number of elements vs. (a) average von Mises stress and (b) scratch depth.

2.5. Artificial Neural Network Approach

Developing a model to predict the material removal requires a computerized numerical system to model the complex and nonlinear relationship between the operating parameters and the output. In these simulations, the operating parameters were considered to be scratch load, particle volume fraction, and particle size. To correlate the operating parameters considered in this study with the wear volume, artificial neural networks (ANNs) were employed. The artificial neural network, which has been widely employed across a variety of science and engineering disciplines [73–77] has the capability to model the behaviour of linear and nonlinear systems, which have a high degree of complexity [47].

In this study, the ANN model was developed based on the biological neural network [78]. The biological neural network included small units called neurons receiving electrochemical signals via synapses. The synapses modify the weight of the received signal during learning. In biology, the brain consists of subsystems, and each subsystem consists of a group of neurons [78]. Similarly, the ANN model acts as a brain with subsystems and neurons, which represent ANN layers and neurons, respectively. These neurons link input data to output using synaptic weights.

Among many types of ANNs, a multilayer perceptron network (MLP) is more common and has been used previously in nonlinear problems (e.g., corrosion [79], erosion [80]). MLP generally consists of an input layer, hidden layers, and an output layer, as shown in Fig. 4. According to other investigators, one hidden layer is usually sufficient to predict the actual output with acceptable accuracy [80, 81]. The number of neurons in the hidden layer is determined by a trial and error approach based on the mean square criterion [83]. In an ANN model, each input is weighed between 0 and 1. The closer the weight to 1, the more significant the input is. The sum of all of the signals' weights consists of the net value of the neurons. Each neuron is also set to a number that corresponds to a threshold over which the neuron will transfer the signal to another neuron. This signal transfer happens if the net value exceeds the neuron threshold. Thus, the generalized knowledge gained in the training process is memorized in terms of the weight of the signals [83, 84].

In MLP, the data is split into training data and test data. Training is the act of continuously adjusting the signal weights until they reach appropriate values that allow the network to closely predict the actual output. The accuracy of the network depends on the weights of these signals.

The training data creates a set of training patterns (x_p, t_p) where p represents the pattern number, x_p and t_p are the input vector pattern and the desired output for the p^{th} training pattern. The input to the j^{th} hidden neuron, $net_p(j)$, is defined as [86]:

$$net_p(j) = \sum_{k=1}^{N+1} W_{hi}(k,j) x_p(k) \quad 1 \le j \le N_h , \tag{17}$$

where $W_{hi}(k,j)$ is the weights connecting the k^{th} input to the j^{th} hidden neuron and subscript k is used to show N input neurons.

The output activation for the p^{th} training pattern ($O_p(j)$) is expressed as:

$$O_p(j) = f(net_p(j)). \tag{18}$$

The sigmoid function is typically chosen as the nonlinear activation function as [83]:

$$f(net_p(j)) = \frac{1}{1+e^{-net_p(j)}}. \tag{19}$$

The overall performance of MLP is calculated by the mean square error (MSE) as follows:

$$E = \frac{1}{N_v}\sum_{p=1}^{N_v} E_p = \frac{1}{N_v}\sum_{p=1}^{N_v}\sum_{i=1}^{M}\left[t_p(i) - y_p(i)\right]^2 , \tag{20}$$

where, N_v is the number of training patterns, the i^{th} output for the p^{th} training pattern can be defined as:

$$y_p(i) = \sum_{k=1}^{N+1} W_{hi}(k,j)\cdot x_p(k) + \sum_{j=1}^{N_h} W_{oh}(i,j)\cdot O_p(j), \tag{21}$$

where $W_{hi}(k, j)$ denotes the weights from input to output neurons and $W_{oh}(i, j)$ the weights from hidden to output neurons.

In this study, $i = M = 1$, the ANN model had just one output, which was the volume loss, and the input layer consisted of WC particle volume fraction, size, and scratch load. The ANN model was developed to correlate these inputs and output using a Matlab® code.

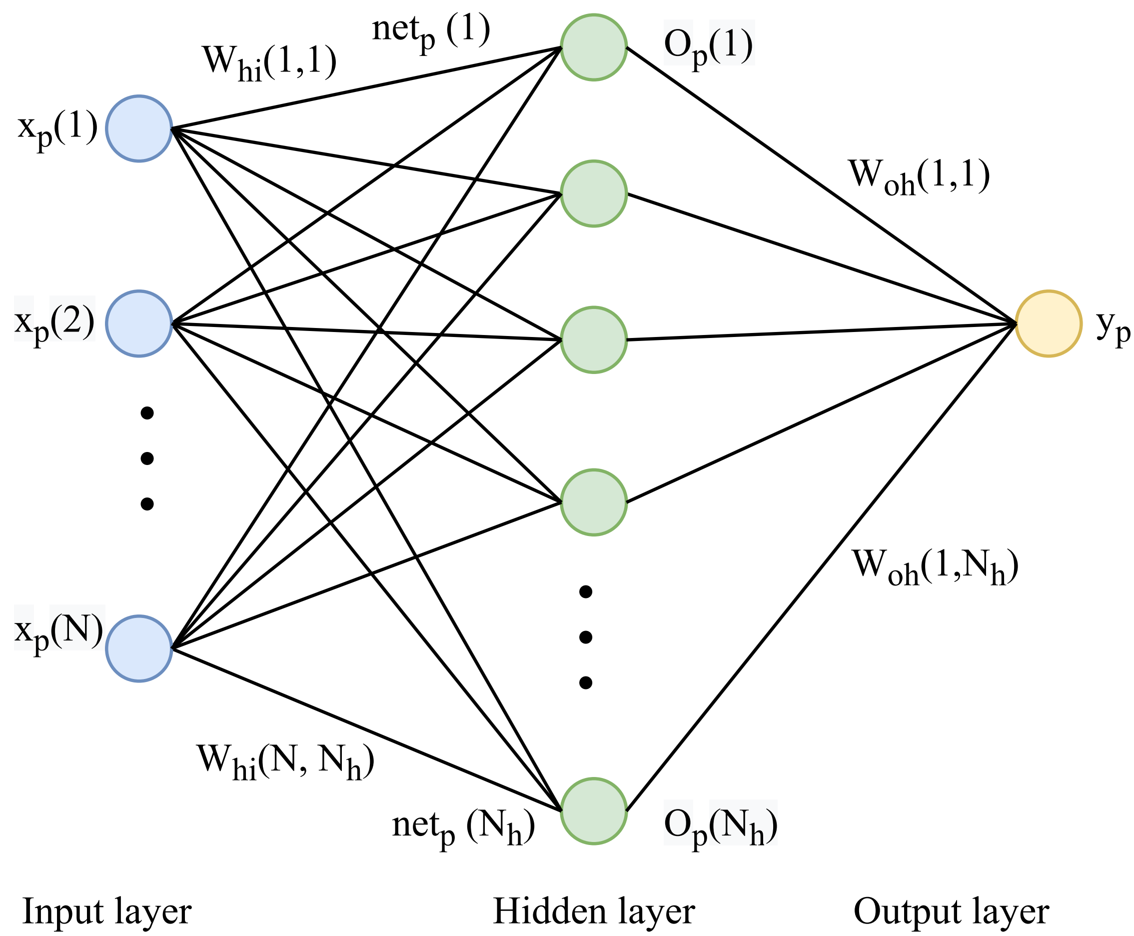

Fig. 4 Topology of an artificial neural network.

3. Results and Discussion

Initially, a scratch test was simulated under progressive load increasing from 0.1 to 30 N to validate the FE scratch model, and the result was compared with the experimental result obtained in the study buy Ul-Hamid, *et al*. [52], as shown in Fig 5. Simulating the scratch test under progressive load facilitated examination of the validity of the FE model. As expected, the scratch depth increased with increasing the load in both experiment and simulation. Although the uncertainty of the study by Ul-Hamid, *et al*. [52] was not given, the scratch depth result obtained using the FE scratch model showed a good agreement with the experimental result in Fig. 5.

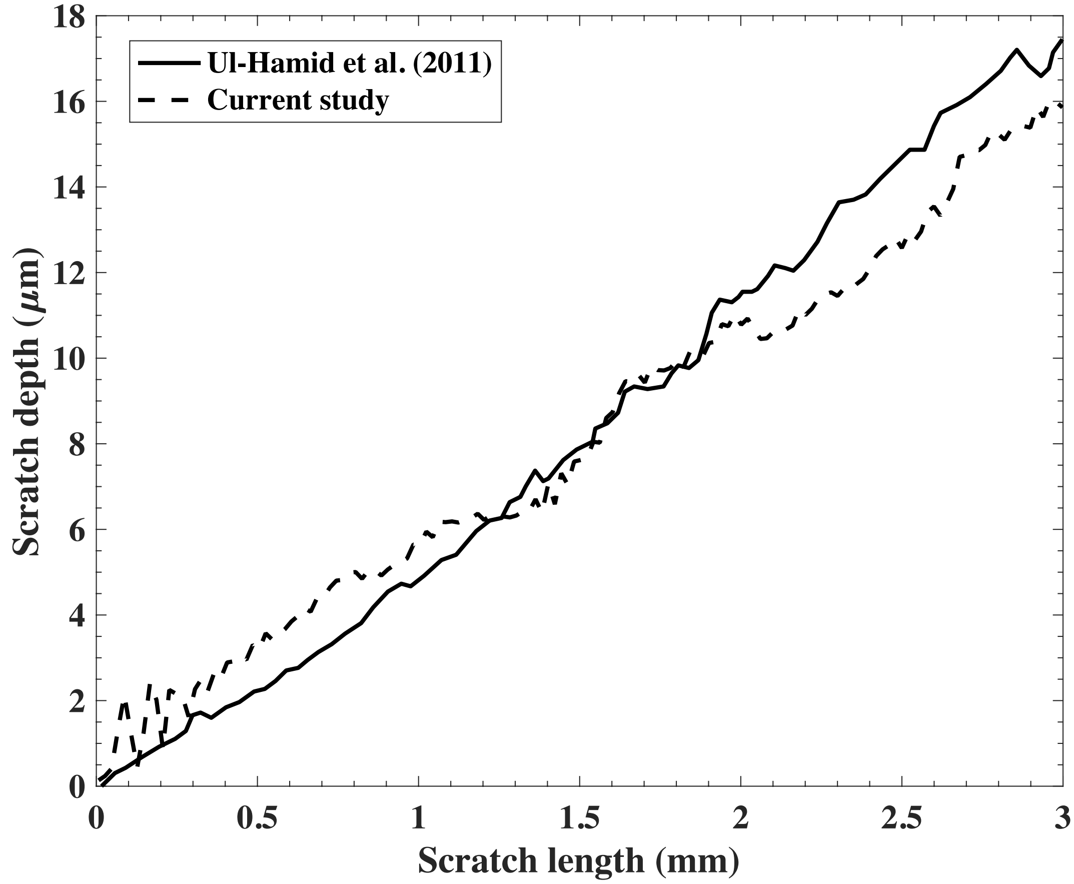

Fig. 5 The scratch length vs. scratch depth comparison between the present model and UI-Hamid, *et al*. experimental study [52].

3.1. Simulation of Residual Stress and Displacement

The contours of stress and displacement will be presented to illustrate the spatial distribution of deformation in the material following a scratch test. This was done by varying the load (1 N to 9 N), particle size (60 μm to 220 μm), and volume concentrations (10 Vol.% to 50 Vol.%). These were shown to see how mechanisms change and evolve as a function of these internal/external parameters. During sliding of the indenter, the shear force was created on the surface of the material, which caused the uppermost layer of the material to be compressed, as shown in Fig. 6. Depending on the size of this shear force, different material removal mechanisms could become dominant [86, 87]. At a scratch load of $1\ \mathrm{N}$, the WC particles deposited in the matrix were the only ones that contributed to the stress distribution (see Fig. 6 (a-I)) and composite hardness and material removal mechanism. The load on the indenter caused the stress is distributed in the substrate and the material is plastically deformed and accumulated on the side of the groove when $\phi = 10$ Vol.% as shown in Fig. 6 (a-II). This is referred to as "microploughing" and this mechanism was also reported by Xiao, *et al*. [87] as the dominant mechanism of material removal at small loads. When increasing the particle volume fraction to 50 Vol.% with the same scratch load, the stress was concentrated at the interface of the particle. The mismatch in properties between the matrix and the reinforcing particles at the interfaces [24] induced large stresses under loading, which resulted in fragmentation and material removal, as shown in Fig. 6 (b-II). Increasing the WC particle volume fraction, which makes the composite brittle [32], may explain this small amount of material removal. In Fig. 6 (b), no clear plastic deformation was observed in the matrix through the surface of the particles due to the protective role of the particles on the matrix. This protective role of the WC particles was also observed in an experimental study by Cao, *et al*. [89].

The residual damage in the substrate was investigated to probe potential damage accumulation and micro-fatigue mechanisms [90]. Typically, the stress was stored in both the matrix and particles at the scratch load of $1\ \mathrm{N}$. The load caused the damage parameter represented in Eq. (2) is increased in each element. This parameter illustrated for the WC particles size of 60 and $140\ \mu\mathrm{m}$ in Fig. 7 revealed that the damage parameter is relatively small (smaller than 0.5) in all the elements, which means that the reinforcing particles may not be significantly damaged even if the scratch test had been repeated, and the stress would have been stored in the form of microfatigue.

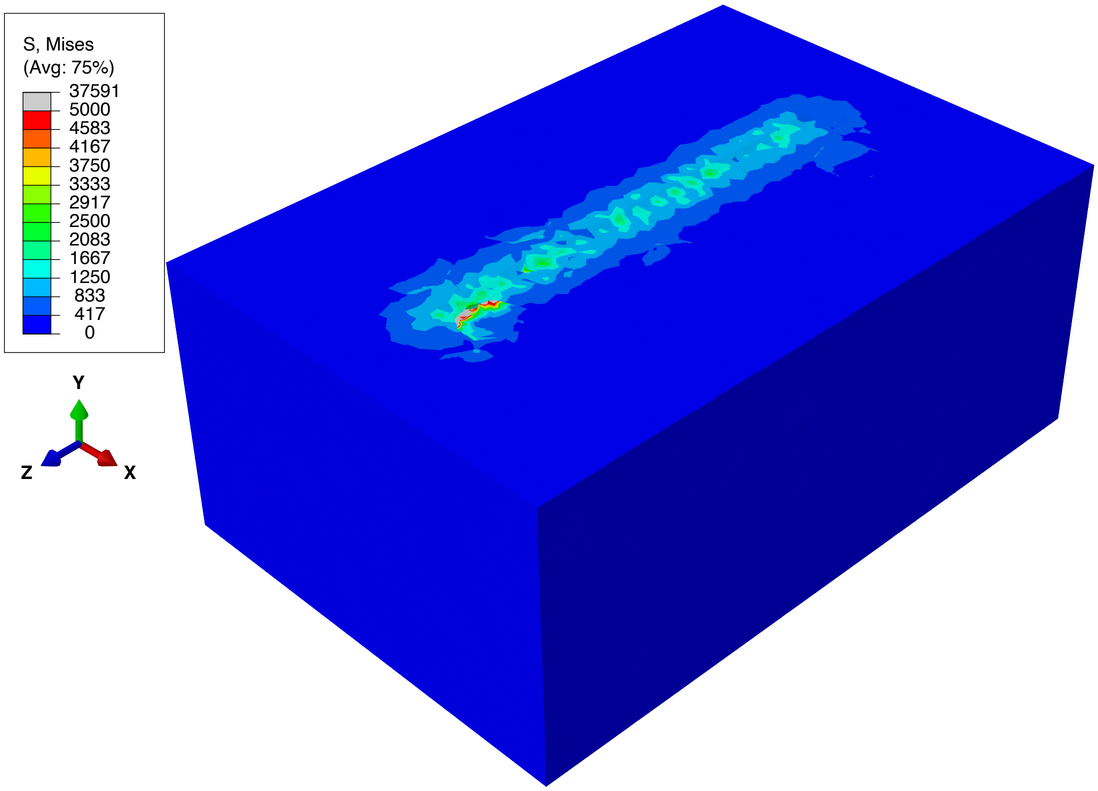
S, Mises
(Avg: 75%)
37591
5000
4583
4167
3750
3333
2917
2500
2083
1667
1250
833
417
0
Y
Z
X

(a-I)


U, U2
0.0009
0.0006
0.0004
0.0001
−0.0001
−0.0003
−0.0006
−0.0008
−0.0010
−0.0013
−0.0015
−0.0018
−0.0020
−0.0026
Z
Y
X

(a-II)

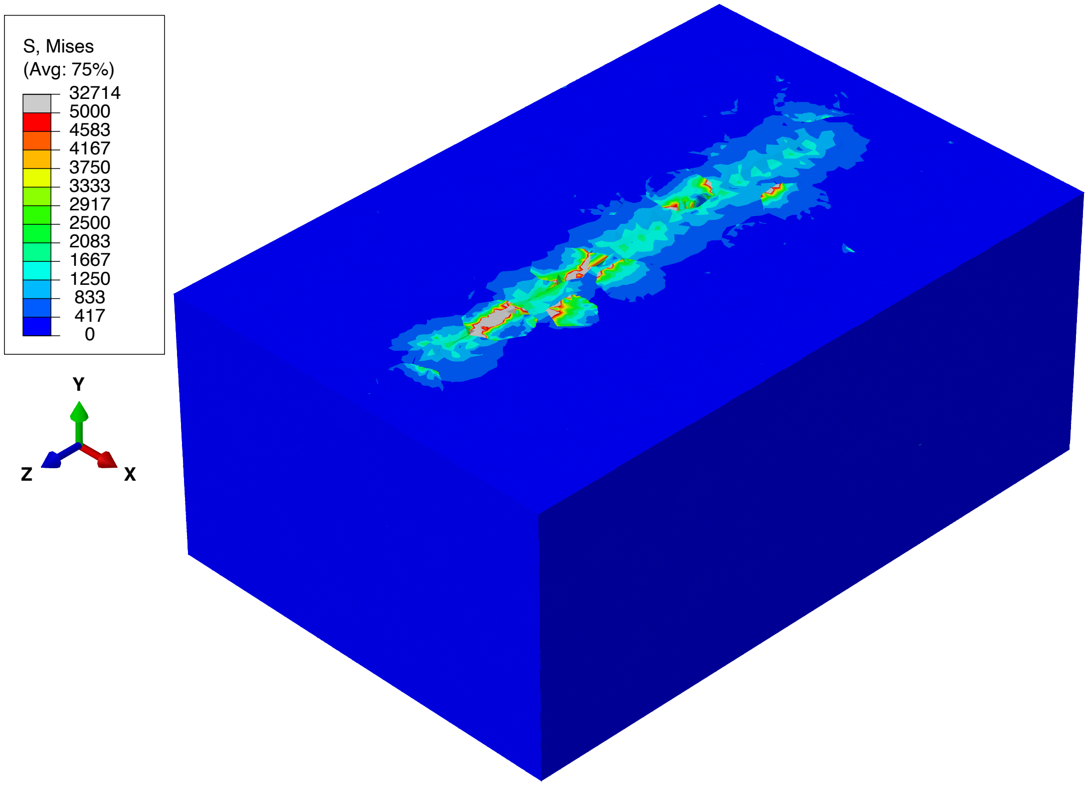
S, Mises
(Avg: 75%)
32714
5000
4583
4167
3750
3333
2917
2500
2083
1667
1250
833
417
0
Y
Z
X

(b-I)

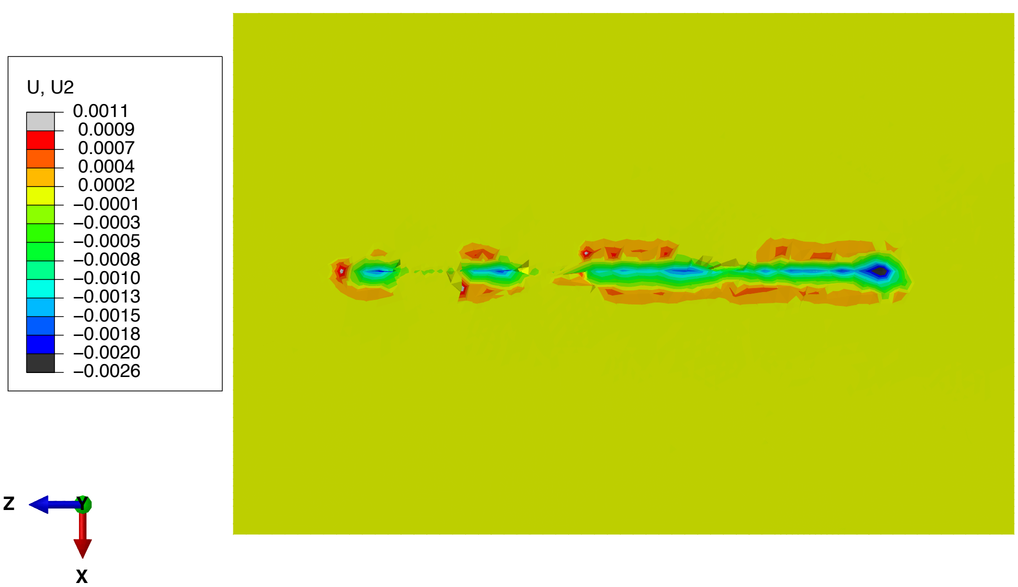
U, U2
0.0011
0.0009
0.0007
0.0004
0.0002
−0.0001
−0.0003
−0.0005
−0.0008
−0.0010
−0.0013
−0.0015
−0.0018
−0.0020
−0.0026
Z
Y
X

(b-II)

Fig. 6 (I) Residual stress (MPa) and (II) displacement (mm) contours of WC-Ni composite coating with WC particle size of 60 μm and (a) ϕ = 10 Vol.% and (b) ϕ = 50 Vol.%, at Load = 1 N .

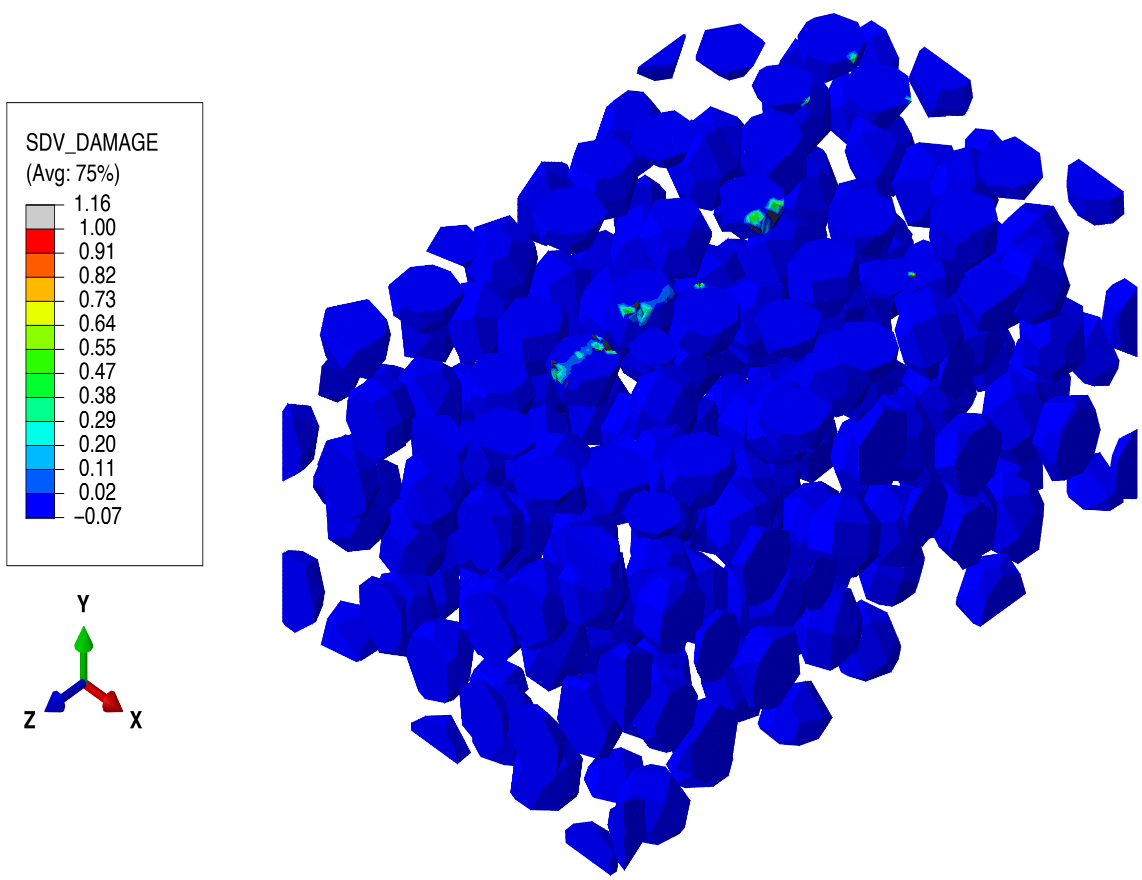

(a)

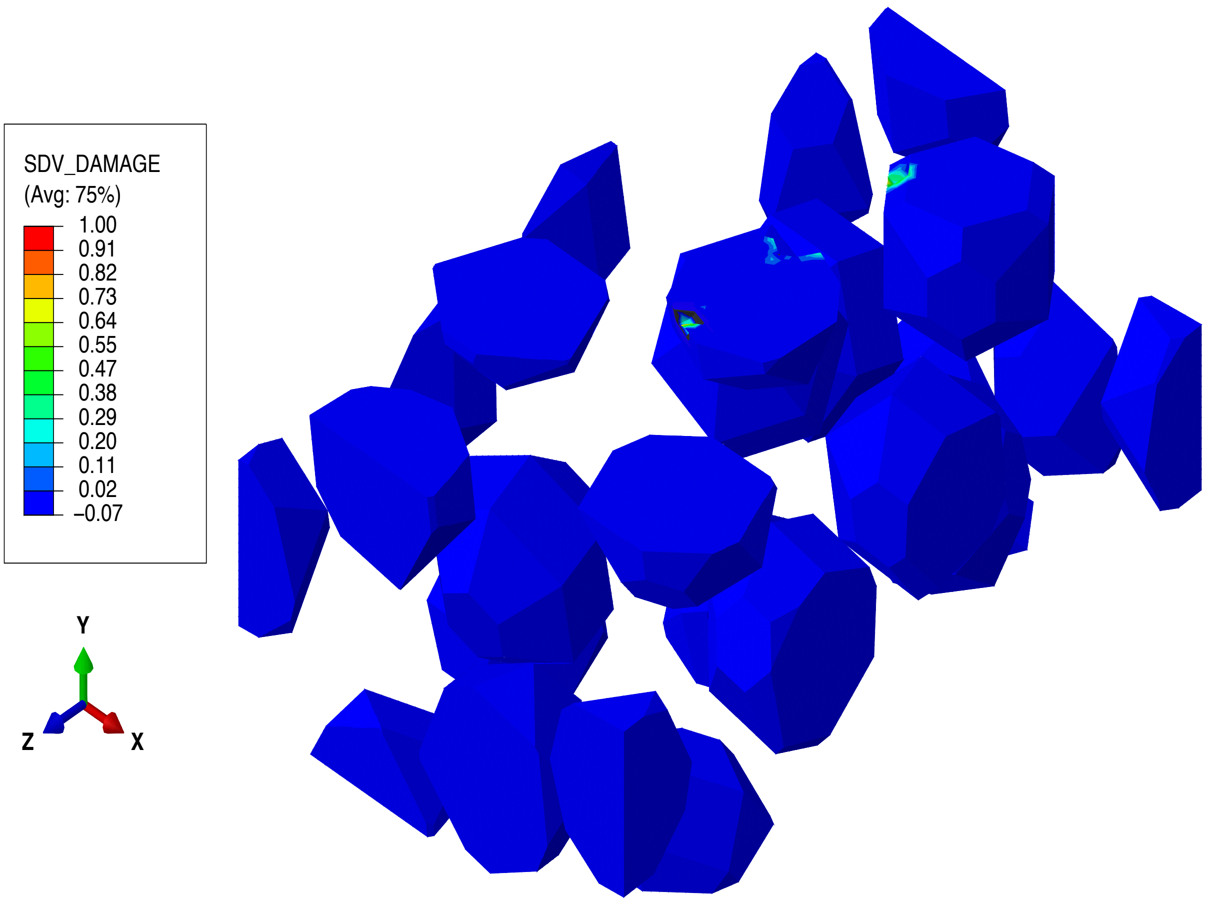

(b)

Fig. 7 Damage parameter contour of the composite coating under 1 N scratch load with 50 Vol.% WC particle content and the diameter of (a) 60 μm and (b) 140 μm.

The stress and displacement contours were also evaluated for the volume fraction of 10 Vol.% at 9 N, as shown in Fig. 8 (a). At this load, the stress was less homogeneously distributed at the volume fraction of 10 Vol.% than the case with 50 Vol.% volume fraction. This could be due to the larger mean free path [91] between the carbide particles [24], which caused the particles that were farther from the groove to undergo lower stresses than the same case with 50 Vol.% (See

Fig. 8 (a-I, c-I)) and the deformation and damage occur quite freely due to the weak resisting role of the reinforcing particles to deformation (See Fig 8 (a-II)). Increasing the particle size from 60 to 140 μm and larger caused the mean free path to become even larger, which caused the plastic deformation to occur in the matrix during sliding even at large volume fractions (i.e., $\phi = 50$ Vol.%). In the case of large WC particle reinforcement, the stress simulated in the composite coating with 10 Vol.% WC particles was greatly affected by the behaviour of the matrix with limited WC particle interference, as shown in Fig. 8 (b). By increasing the particle volume fraction to 50 Vol.% (see Fig. 8 (c)), the mean free path decreased, which caused the material surrounded by the WC particles to be forced laterally and the vertical flow of the matrix between the WC particles was reduced. Also, the higher volume fraction caused the stress to be distributed more uniformly in the composite coating, as shown in Fig. 8 (c-I). This is because the local load can be more easily transferred to the adjacent particles due to the smaller mean free path. This smaller mean free path caused transfer of stress to the particles and matrix, and the particles located further from the groove experienced larger residual stresses than the case with the same particle size and volume fraction of 10 Vol.%, as illustrated in Fig. 8 (c-I). Also, the composite revealed severe deformation in the areas surrounded by WC particles, as shown in Fig. 8 (c-I). This deformation related to the presence of the WC particles was also observed in a study conducted by Varga*, et al*. [40].

Increasing the particle volume fraction affected the material removal mechanism. The material removal mechanism changed from microploughing to microcutting with increasing the particle volume fraction from 10 to 50 Vol.%, as less matrix deformation and accumulation on the side of the groove was observed in Fig. 8 (c-II). Instead, a chip was formed in front of the indenter at the end of sliding. This chip formation in front of the indenter was also observed in the scratch experiment conducted by Tkaya *et al.* [88], where the microcutting mechanism was dominant.

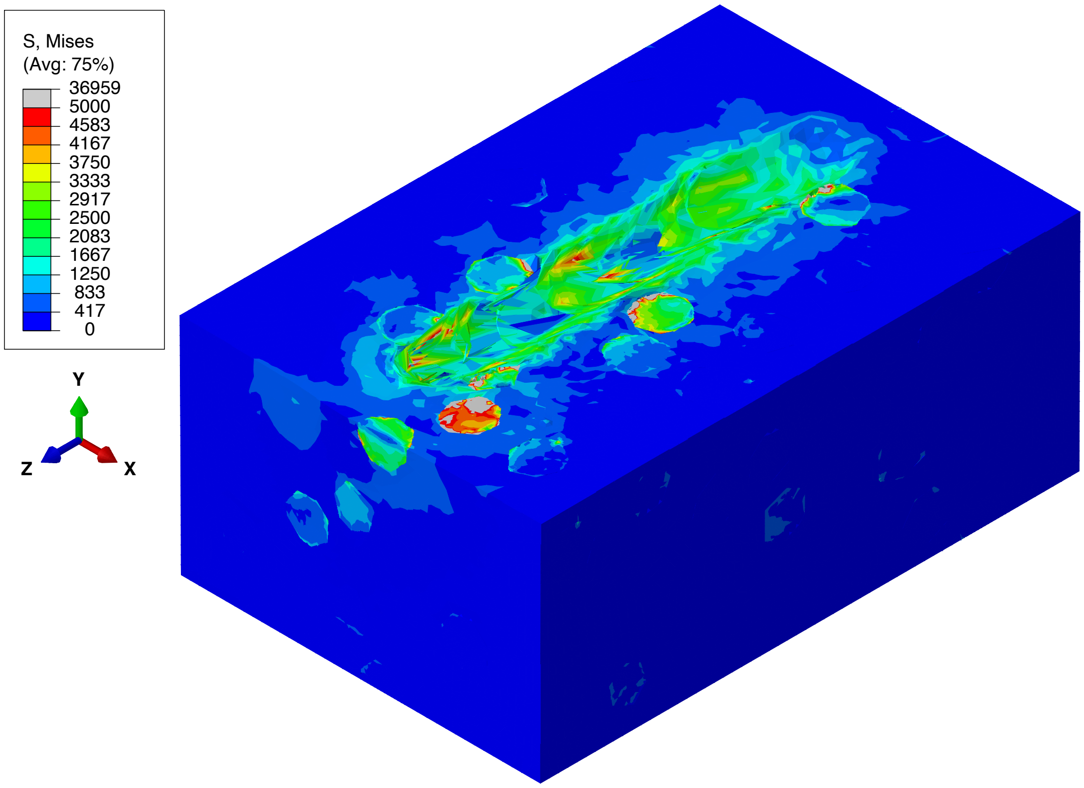
S, Mises
(Avg: 75%)
36959
5000
4583
4167
3750
3333
2917
2500
2083
1667
1250
833
417
0
Y
Z
X

(a-I)

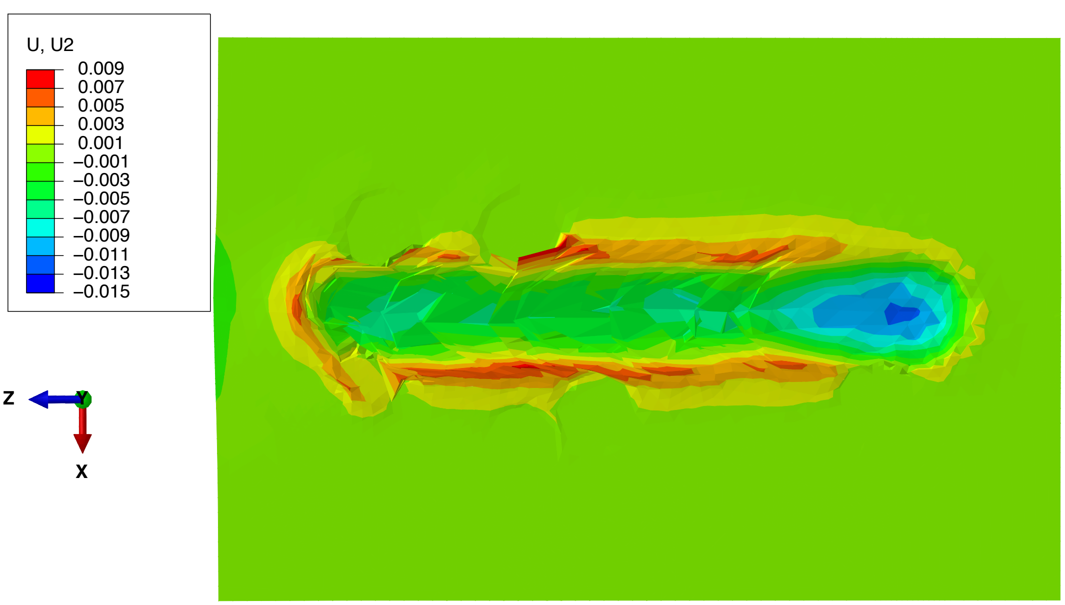
U, U2
0.009
0.007
0.005
0.003
0.001
−0.001
−0.003
−0.005
−0.007
−0.009
−0.011
−0.013
−0.015
Z
Y
X

(a-II)

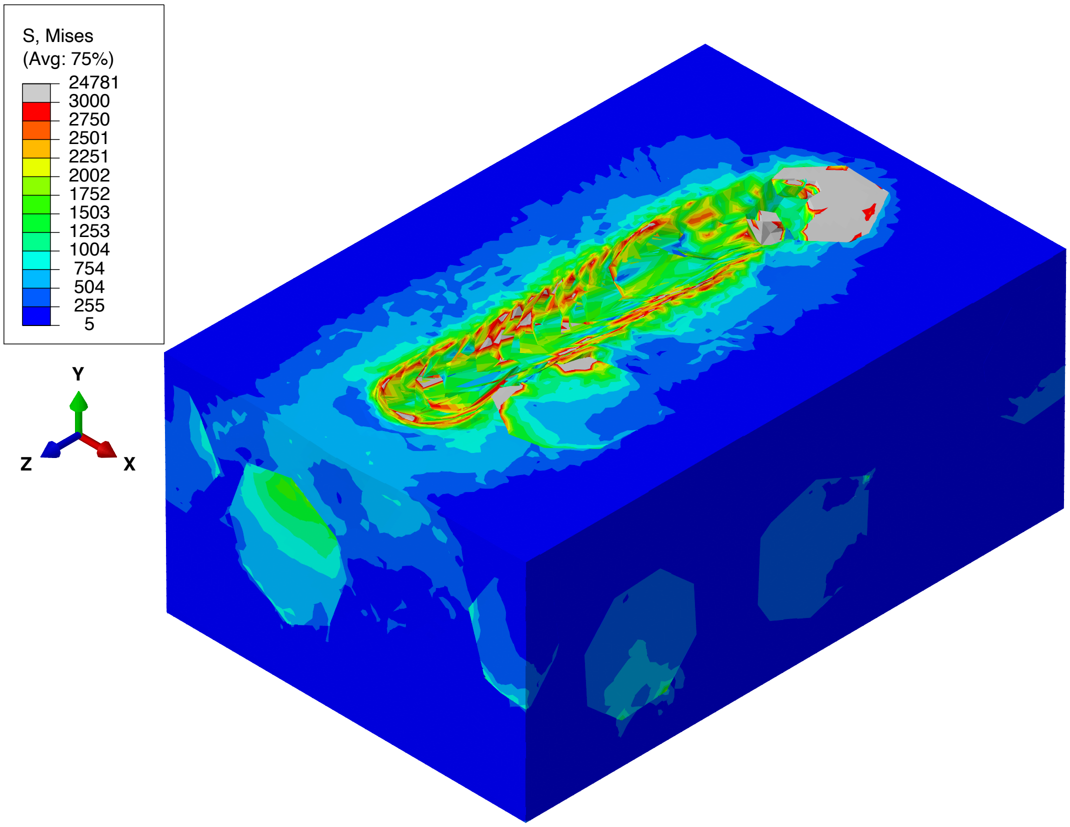
S, Mises
(Avg: 75%)
24781
3000
2750
2501
2251
2002
1752
1503
1253
1004
754
504
255
5
Y
Z
X

(b-I)

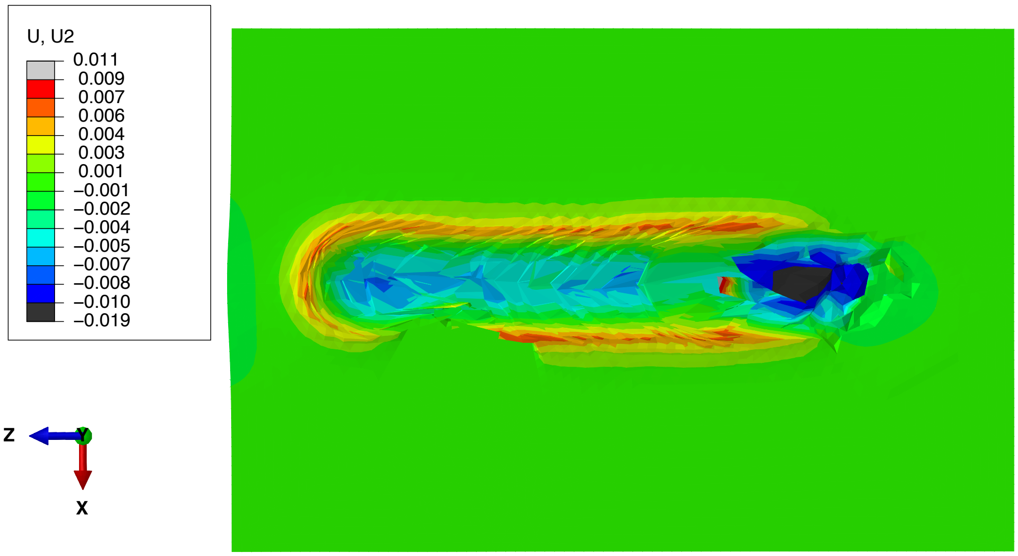
U, U2
0.011
0.009
0.007
0.006
0.004
0.003
0.001
−0.001
−0.002
−0.004
−0.005
−0.007
−0.008
−0.010
−0.019
Z
X

(b-II)

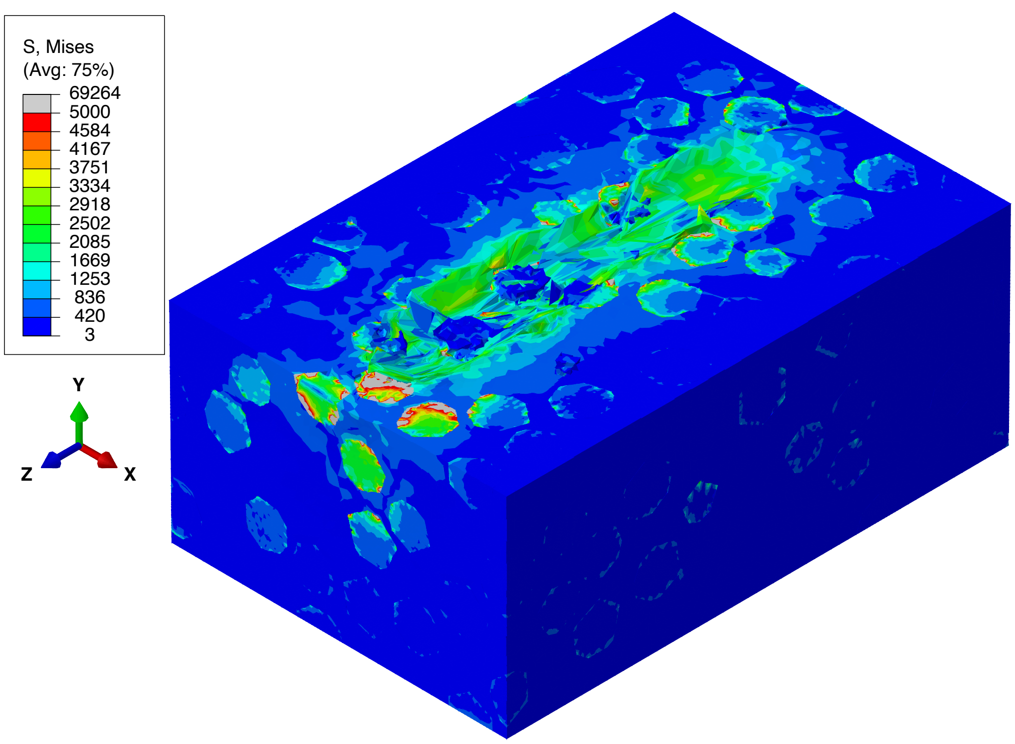
S, Mises
(Avg: 75%)
69264
5000
4584
4167
3751
3334
2918
2502
2085
1669
1253
836
420
3
Y
Z
X

(c-I)

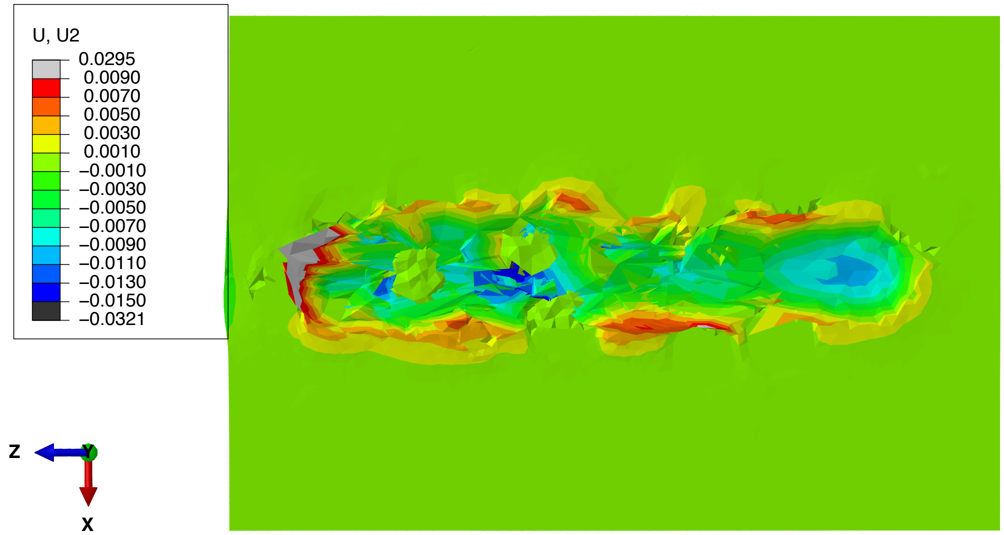

(c-II)

Fig. 8 (I) Residual stress (MPa) and (II) displacement (mm) contours of WC-Ni composite coating at (a) $d_p = 60\ \mu m$, $\phi = 10$ Vol.%, Load = 9 N, (b) $d_p = 140\ \mu m$, $\phi = 10$ Vol.%, Load = 9 N, and (c) $d_p = 60\ \mu m$, $\phi = 50$ Vol.%, Load = 9 N.

3.2. Maximum Principal Stress Distribution

To better understand the effects of the WC particles on the scratch resistance of the composite coating and strengthening mechanisms of the composite, the evolution of the maximum principal stress field was determined in the cross-section of the composite along the *z*-axis for three different particles sizes (i.e., 60, 140, and 220 μm). The results are shown in Fig. 9. The stress in the particles was much larger than those in the matrix, which revealed that a larger load was carried by the particles and highlighted the load-carrying role of the particles in the composite [92]. The stress was more homogeneously dispersed in the smaller particles than in those that were larger (see Fig. 9). This facilitated transfer of the stresses to adjacent particles and led to uniform stress distribution in the composite. This stress distribution could be in the form of compression stress, which happened in front of the indenter, and tensile stress, which happened behind the indenter, as shown in Fig. 9. Stress concentration was also observed at the interface of the matrix and the particles, which has been reported to be due to the mechanical properties mismatch between the matrix and particles [24]. This high concentration of stress at the interface may have caused initiation of fractures within the particle and, eventually, material removal.

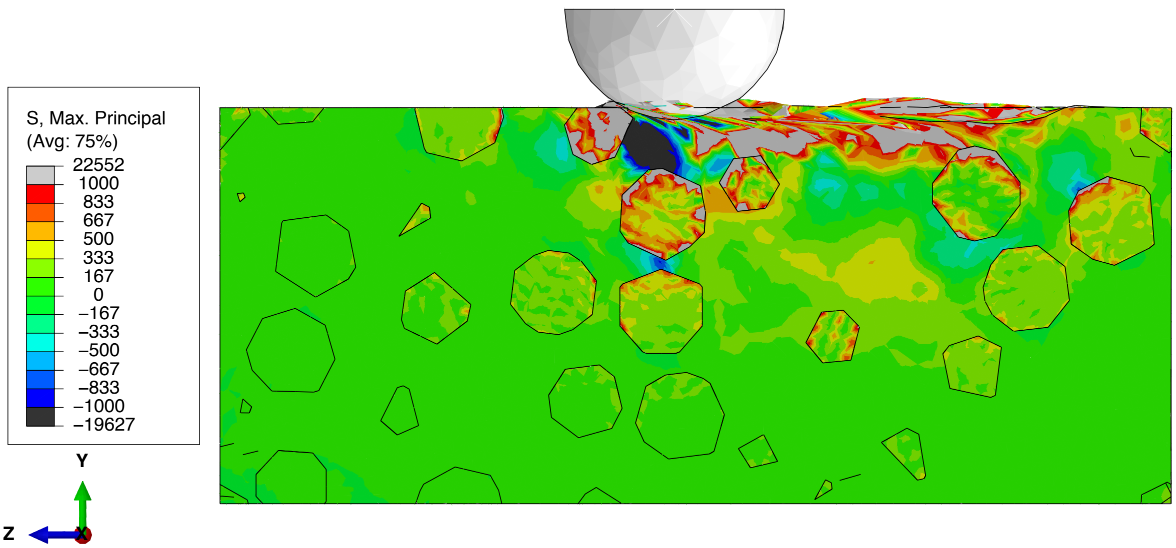

(a)

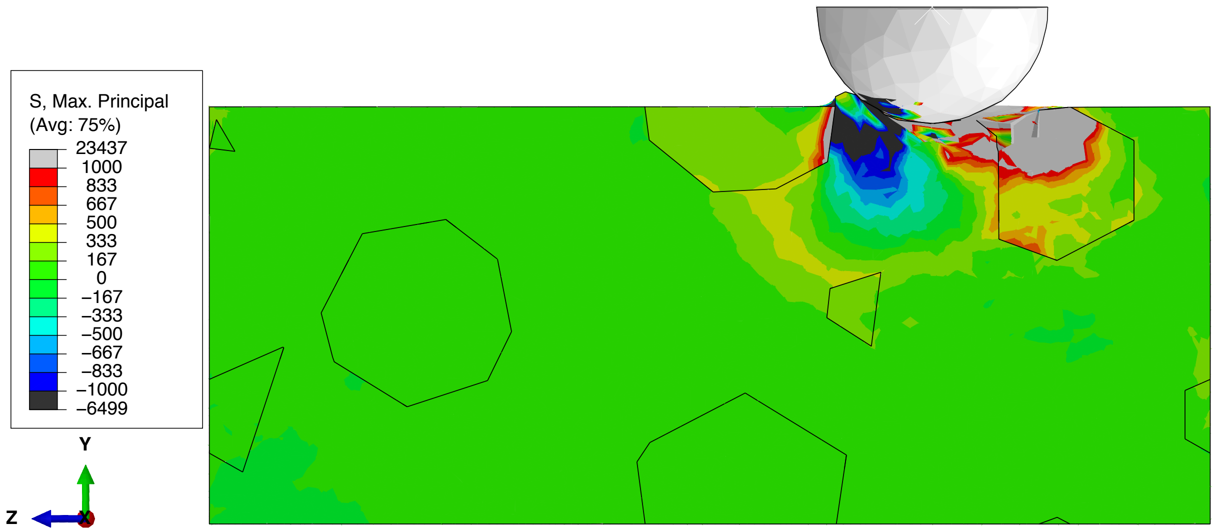

(b)

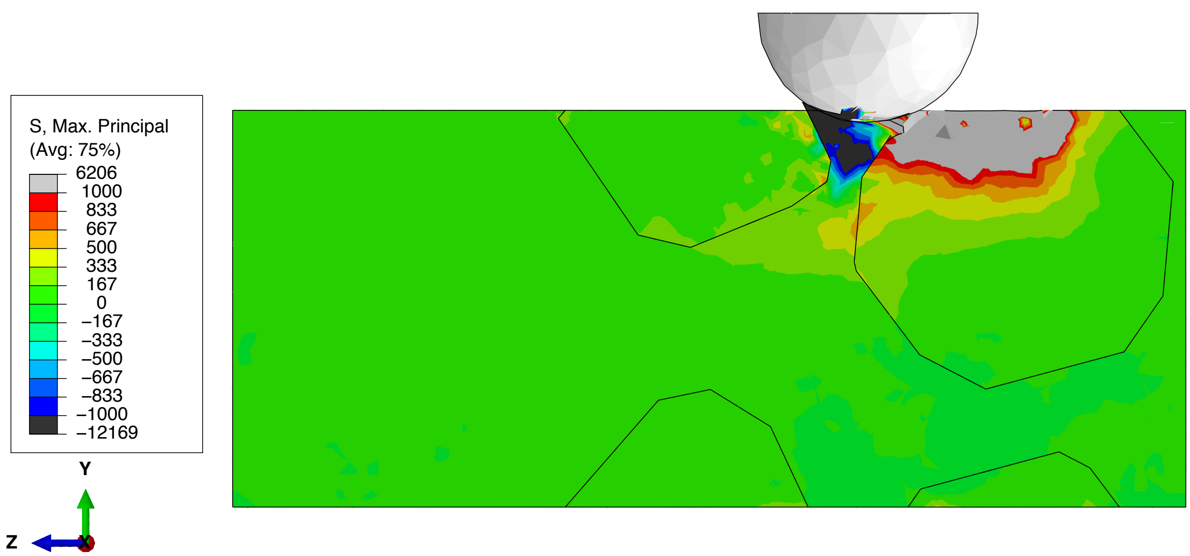

(c)

Fig. 9 Maximum principal stress (MPa) contour of WC-Ni composite coating undergoing a load of 9 N with 50 Vol.% particles and particle size of (a) 60 μm (b) 140 μm, and (c) 220 μm.

3.3. Scratch Characterization and Mechanical Behaviour

To analyze the effect of WC particle size and volume fraction on the scratch depth, the scratch load was held at $5\ \mathrm{N}$, and the residual scratch depth of the composite coatings and the Ni substrate, with no reinforcing particles, was obtained over the geometry, as shown in Fig. 10. Regardless of the size and the volume fraction of the WC particles, the scratch depth was reduced when adding WC particles. This reduction of scratch depth was not monotonic along the scratch length due to the presence of the WC particles, particularly when the WC particle's volume fraction was $30\ \mathrm{Vol.\%}$ and higher and the particle size was $140\ \mu\mathrm{m}$ and larger. The reinforcing particles impeded penetration of the indenter into the MMC coating. This was the reason for this non-monotonic reduction of the residual scratch depth, which was previously reported in studies by Hu, *et al*. [44, 45].

During sliding of the indenter over the composite coating, the scratch load induced material removal and wear, resulting in worn volume loss. The worn volume loss of the Ni substrate with no reinforcement increased from nearly $300\ \mu\mathrm{m}^3$ to $4.5\times10^5\ \mu\mathrm{m}^3$ by increasing the scratch load from $1\ \mathrm{N}$ to $9\ \mathrm{N}$, as shown in Fig. 11. At a scratch load of $1\ \mathrm{N}$, the material from the Ni substrate with no reinforcing particles was removed mainly after plastic deformation, and the worn volume was negligible, as shown in Fig. 11 (a). This negligible material removal with a scratch load of 1 N was also reported in a study by Xiao, *et al.* [87]. By increasing the scratch load, the material that was removed increased considerably (See Fig. 11 (b)-(c)) due to the domination of the microcutting mechanism during material removal at higher loads [87].

At a scratch load of $1\ \mathrm{N}$ (See Fig. 11 (a)), the role of the microfatigue mechanism on material removal, was more pronounced at small loads. The worn volume loss was slightly reduced with adding 10 Vol.% of WC particles regardless of the size of WC particles. Also, increasing the volume fraction and size of the particles showed an adverse effect on the worn volume. Generally, understanding the effect of WC particle volume fraction on material removal and loss might be difficult at small loads with a single asperity scratch test. With the interaction of one abrasive particle, the stress was mostly stored in the element, and the damage parameter remained smaller than 1. This means that multiple cycles are required to clearly demonstrate the role of reinforcing particles and damage on the composite and their effect on microfatigue [32].

At a scratch load of $5\,\mathrm{N}$ (see Fig. 11(b)), the WC particles improved the wear resistance of the composite compared to the Ni substrate with no WC particle reinforcement. The material resistance varied with changes in the WC particle volume fraction and size due to the competition of two decisive factors, namely hardness of the composite [12, 14, 92] and impeding penetration of the indenter [44, 45]. Larger particles (i.e., 140 and $220\,\mu\mathrm{m}$) than the indenter impeded indenter penetration into the composite better than the smaller WC particles (i.e., $60\ \mu\mathrm{m}$), which has been noted elsewhere by Hu, *et al.* [46], as shown in Fig. 10. As a result, the volume worn by the indenter was reduced when the particle's diameter was 140 and $220\,\mu\mathrm{m}$, as shown in Fig. 11 (b). As noted by Alzouma, *et al*. [17], the larger volume fraction of the WC particles protected the matrix from plastic deformation. With increasing the particle volume fraction, the composite became more brittle [46], which promoted the microcutting mechanism of material removal, with the microfracturing of the WC particles [32]. Thus, with increasing the WC particle volume fraction, the bulk hardness may increase with a tradeoff in toughness. This indicated that a critical WC particle volume fraction exists at which the worn volume is minimum [17, 45], and this is likely related to the competition of hardness and the impeding reinforcing particle effect mentioned earlier (Fig. 11 (b)).

The effects of larger loads on the mechanisms involved in material removal were analyzed by increasing the normal load to $9\ \mathrm{N}$. By increasing the scratch load, the impeding penetration of the indenter due to the larger WC particles was less pronounced, particularly at $\phi = 50$ Vol.%, as the worn volume loss was significantly reduced for any concentration of WC particles when the particle size was $60\ \mu\mathrm{m}$, as shown in Fig. 11 (c). At this time, the particle fracture played a significant role in damage and failure of the composite. The worn volume loss was related to the bulk hardness of the composite, the volume loss decreased with inclusion of smaller WC particles. This reinforcement was reduced due to particle fracture particularly when the particle size was large [94]. The high stress concentration at the edge of large particles was one possible reason for the fracture of brittle particles. Also, the critical volume fraction at which the lowest worn volume loss was observed was dependent on particle size. These changes in the critical volume fraction were also reported elsewhere [17, 45]. This suggests that a strong relationship exists between the scratch load, particle size, and volume fraction, and material loss during loading.

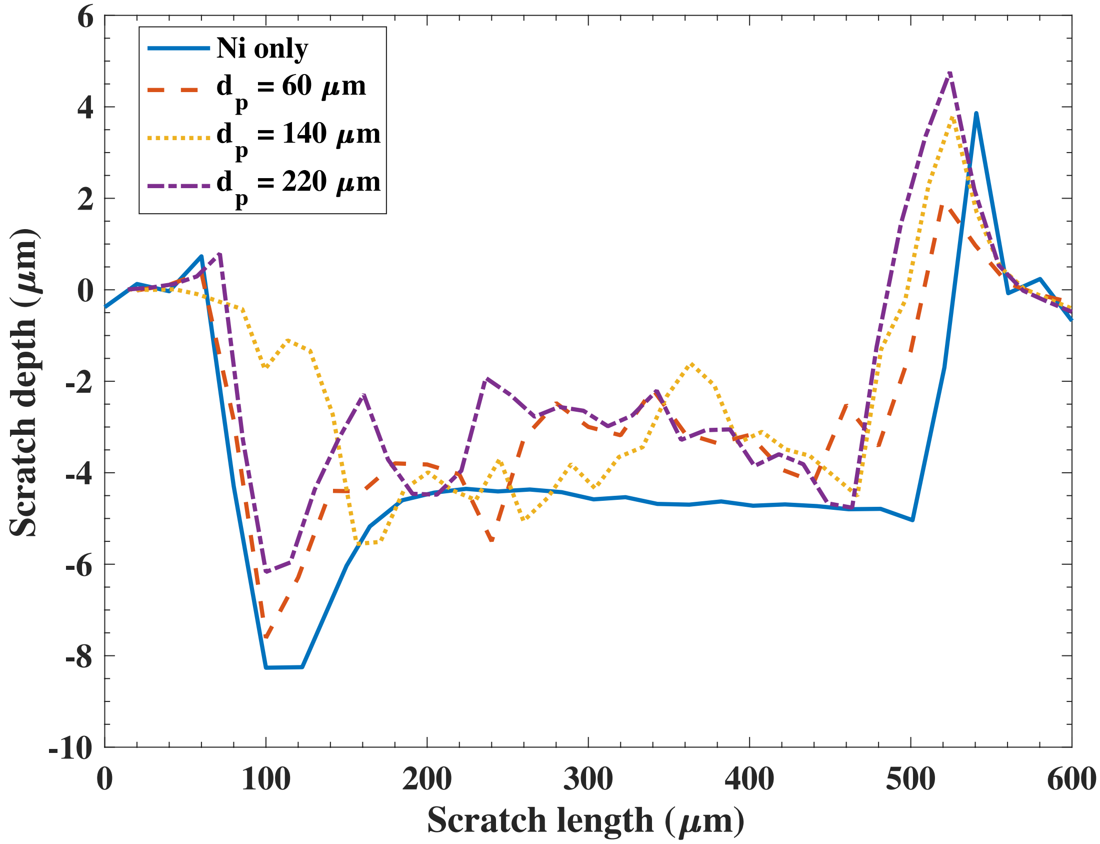
Ni only
d_p = 60 μm
d_p = 140 μm
d_p = 220 μm
6
4
2
0
-2
-4
-6
-8
-10
0
100
200
300
400
500
600
Scratch depth (μm)
Scratch length (μm)

(a)

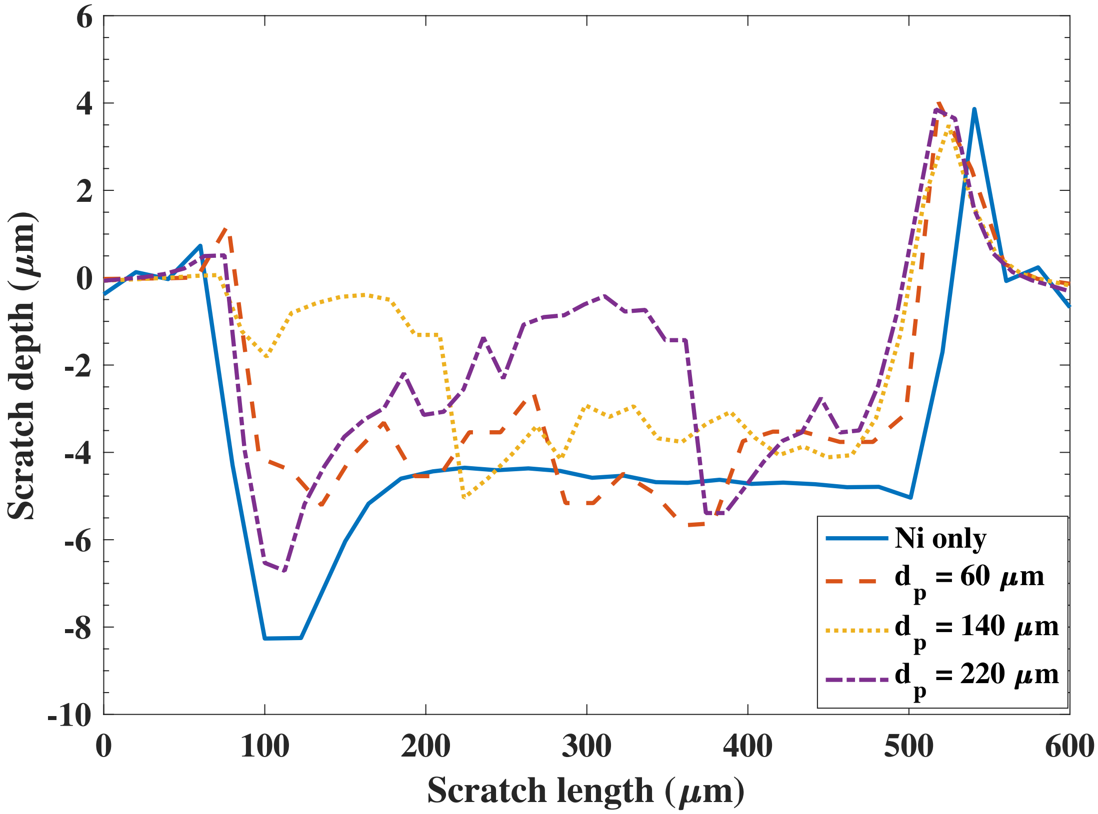
6
4
2
0
-2
-4
-6
-8
-10
Scratch depth (μm)
0
100
200
300
400
500
600
Scratch length (μm)
Ni only
d_p = 60 μm
d_p = 140 μm
d_p = 220 μm

(b)

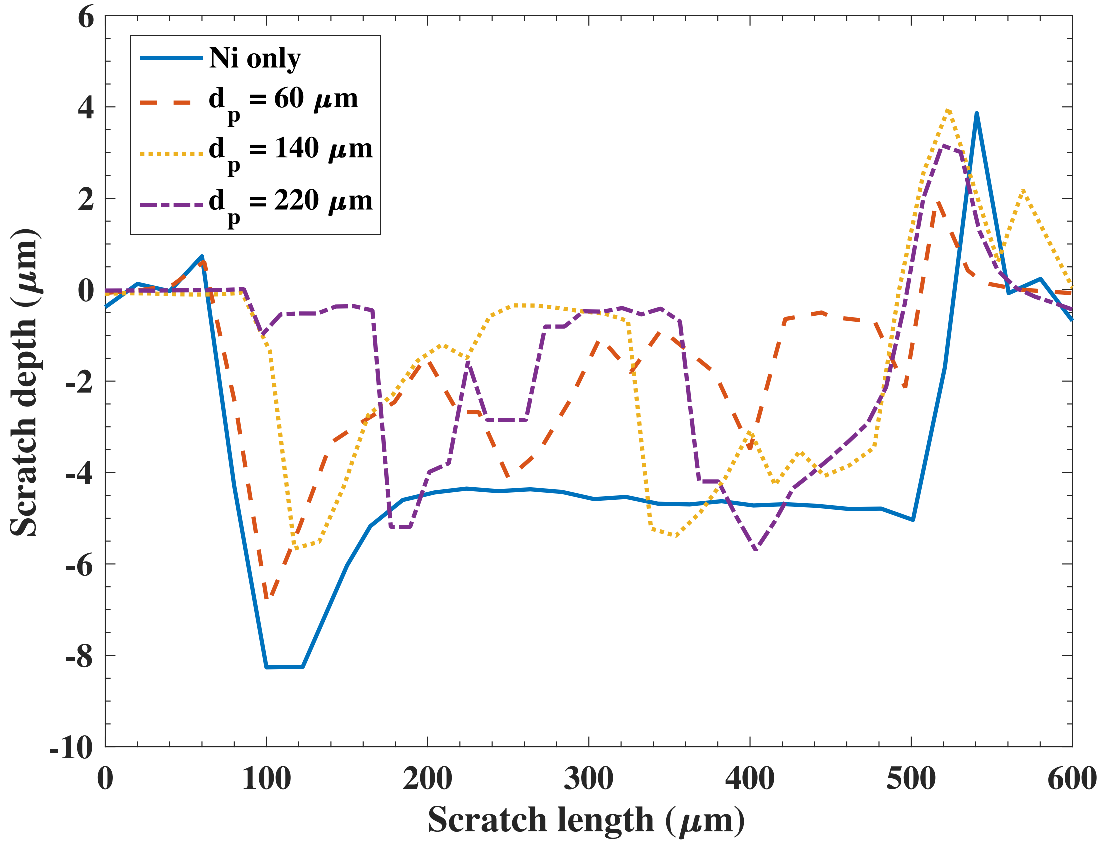

(c)

Fig. 10 Scratch depth vs. scratch length of the Ni and WC-Ni composite coating at the scratch load of 5 N with different WC particle sizes and volume fraction of (a) 10 Vol.%, (b) 30 Vol.%, and (c) 50 Vol.%.

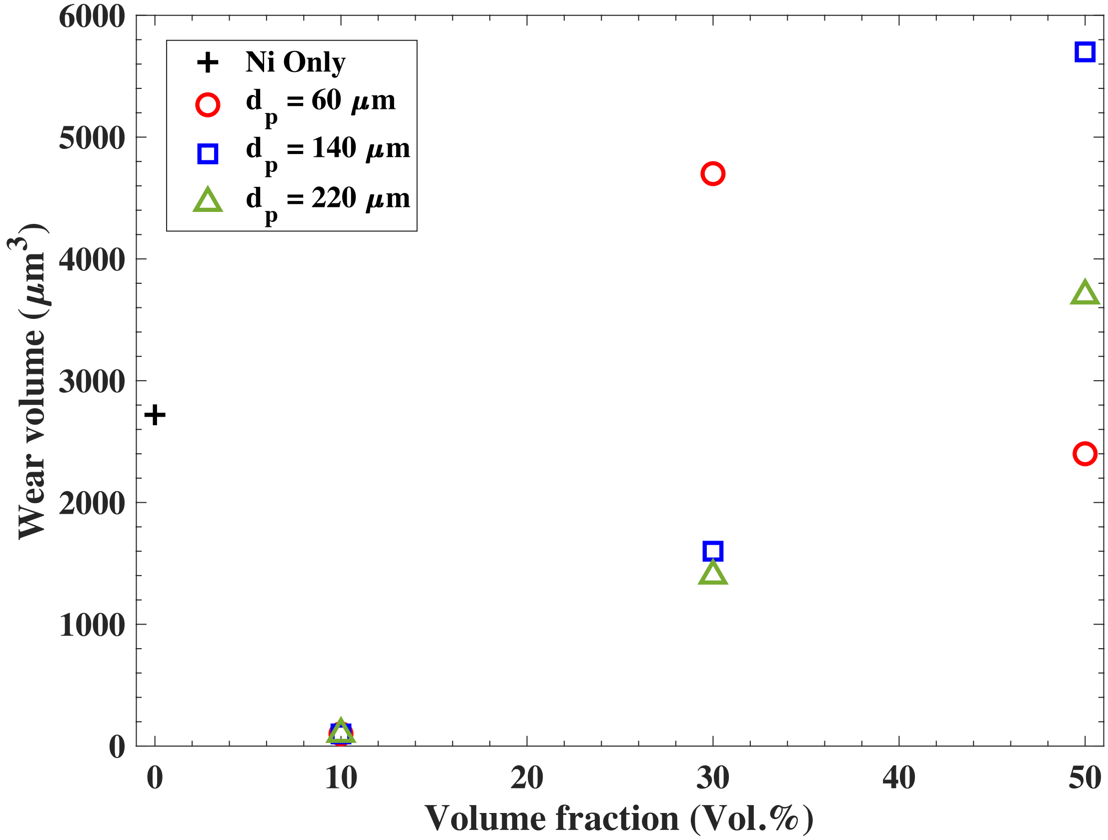
Ni Only
d_p = 60 μm
d_p = 140 μm
d_p = 220 μm
Wear volume (μm^3)
Volume fraction (Vol.%)
0
1000
2000
3000
4000
5000
6000
0
10
20
30
40
50

(a)

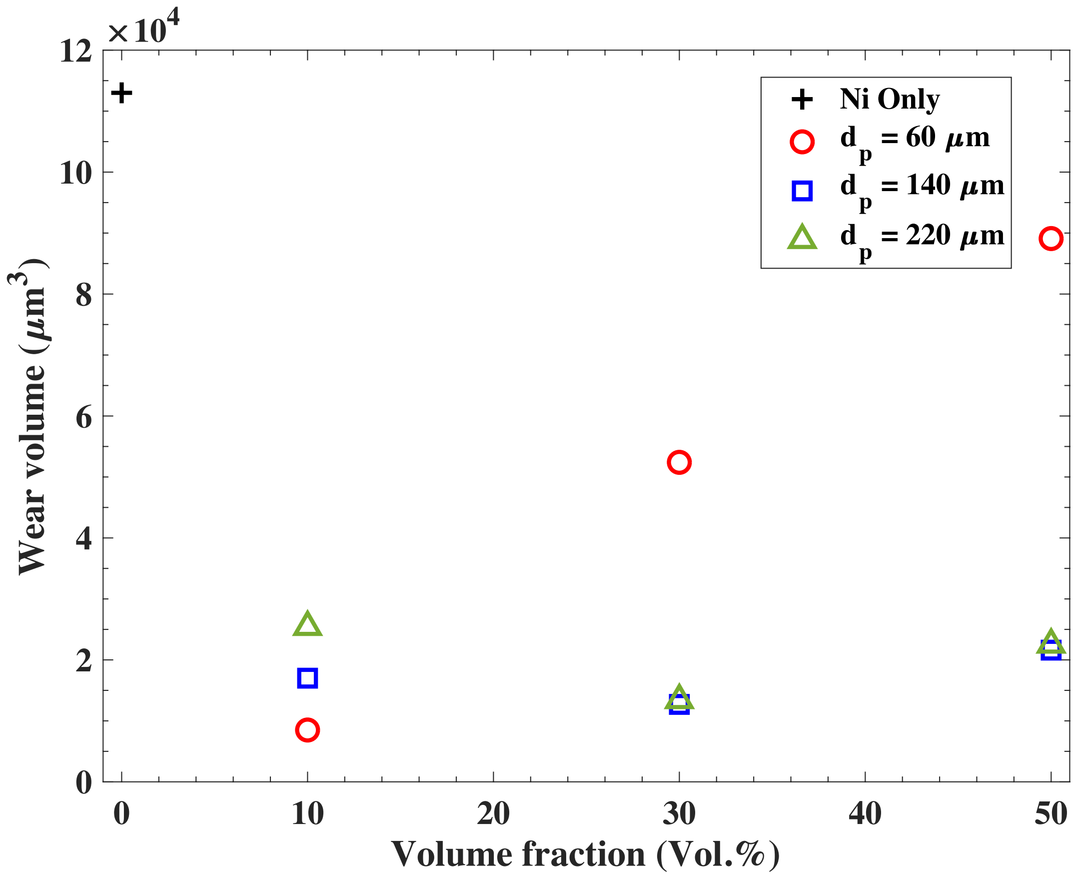
×10^4
12
10
8
6
4
2
0
Wear volume (μm^3)
0
10
20
30
40
50
Volume fraction (Vol.%)
Ni Only
d_p = 60 μm
d_p = 140 μm
d_p = 220 μm

(b)

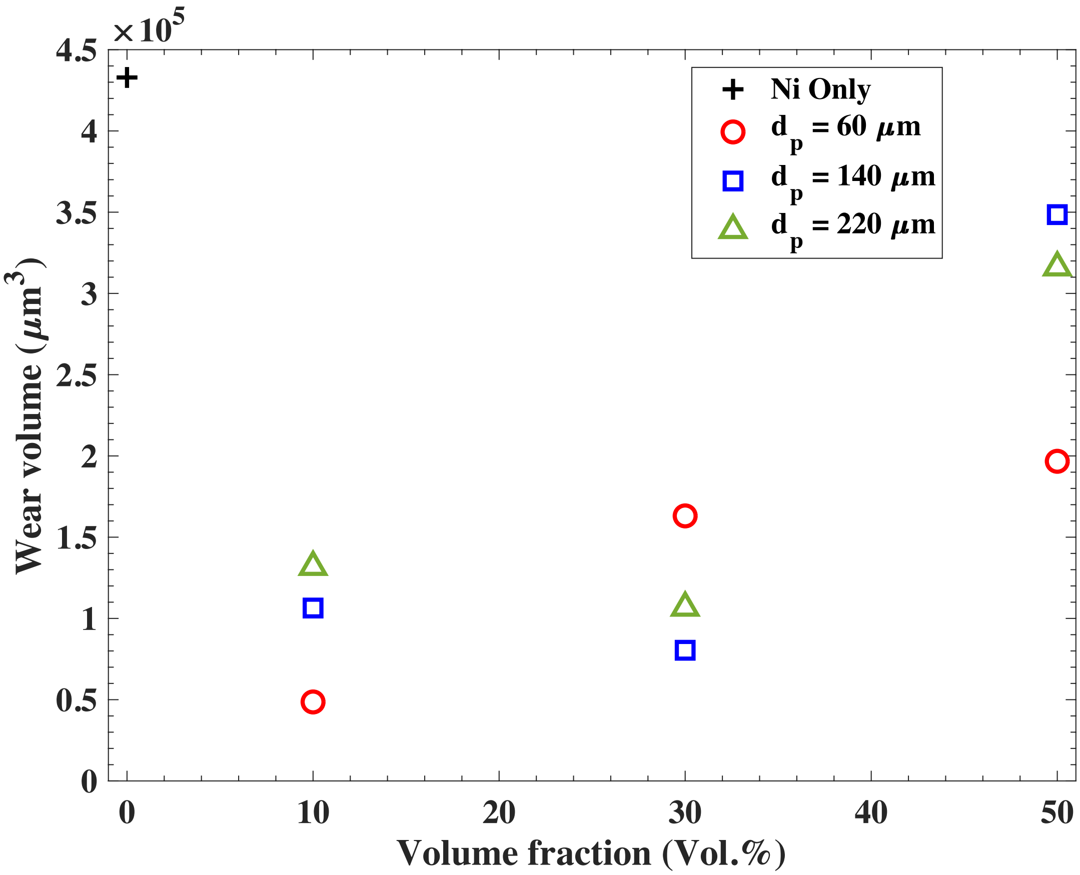

(c)

Fig. 11 Worn volume of all the Ni and the WC-Ni composite coatings with different WC particle size and volume fractions at a normal load of (a) 1 N, (b) 5 N, and (c) 9 N.

3.4. Predictions from ANN Computation Model

An ANN model was developed and trained to predict the worn volume of the composite coating by considering different combinations of scratch load, WC particle size, and volume fraction values. The worn volume was shown for all of these combinations in Fig. 11. In addition, mechanical properties for the matrix and particles were varied by 15 % [95] in order to account for potential variability in the outcomes when generated through this generalized ANN model. Considering this Ni strengthening effect, the worn volume was also obtained for different combinations of the scratch load (1, 5, 9 N), WC particle size (60, 140, and 220 μm), and WC particle volume fraction (10, 30, and 50 Vol.%). The data were randomly categorized into a training set, validation set, and test set. The training and validation sets were employed to train the model for a certain number of neurons in the hidden layer and to optimize the number of neurons in the hidden layer, respectively. For this reason, the model was trained using a hidden layer with 1 to 5 neurons, and the root mean square error (RMSE) [96] was calculated for both training and validation sets, as shown in Fig. 12. It was found from the figure that the lowest RMSE can be obtained in both training and validation sets when the number of neurons is set to 3.

The hidden layer with 3 neurons was chosen to train the model, and the true versus predicted worn volumes of the training and validation data sets were calculated along with the test data set (see Fig. 13), which was not used to train or optimize the number of neurons. The predicted R^2 [96] was found to be 0.965, which demonstrates the accuracy of the model.

Using the proposed ANN model in the industry for evaluating the resistance of the MMC coatings against wear can be beneficial in different aspects. First, reducing the production cost, time-consuming experiments, and the number of expertise to conduct these experiments are some critical benefits of such a model [97]. Second, the proposed model can be used to predict the nonlinear highly complex wear problem of a composite coating with different particle sizes and volume fractions undergoing different normal loads [97, 98].

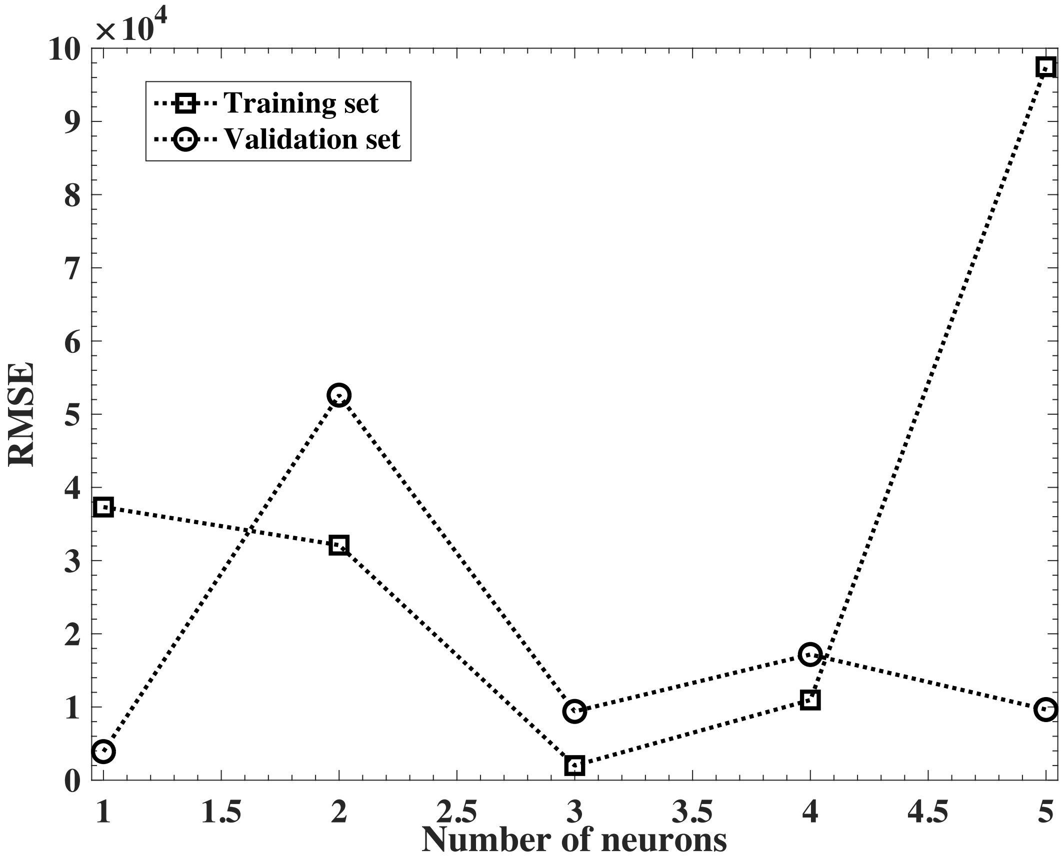

Fig. 12 The number of neurons versus root mean square error for both training and validation data sets.

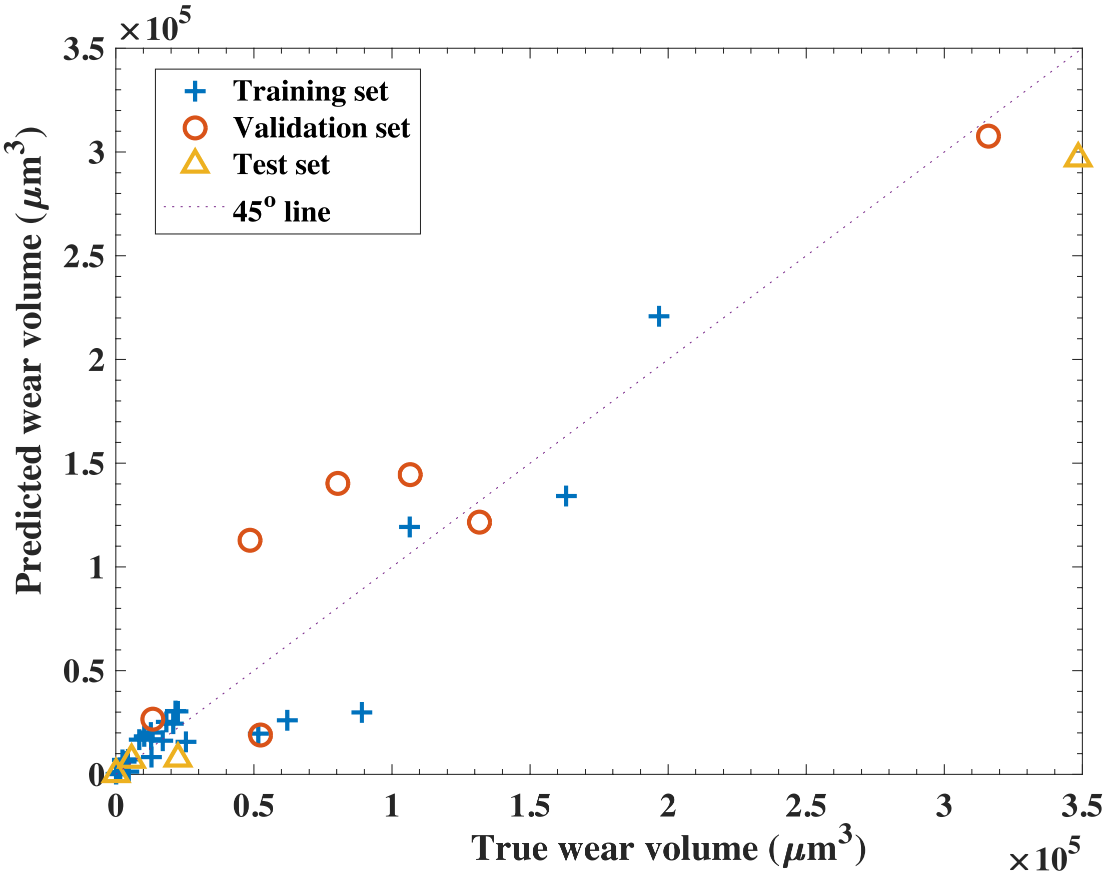

Fig. 13 True wear volume vs. predicted wear volume for all data sets.

4. Conclusions

In this paper, a three-dimensional finite element model was developed to model the scratch test in different WC-Ni composite coatings for ranging WC particle sizes ($60-220\ \mu m^3$) and volume fractions ($10-50$ Vol.%) under different scratch loads ($1-9$ N). The indenter size choice was motivated by the sand size observed in the Albertan oil sands. The Johnson-Cook model and Johnson-Holmquist models were employed to simulate the mechanical behaviour of Ni and WC, respectively. The developed model was validated with the experimental data obtained from the literature, and the scratch test was simulated for a substrate made of Ni with no reinforcing particles. To predict the effects of normal load, WC particles volume fraction and size on the worn volume, the worn volume was calculated for each combination of these parameters, and an ANN model was trained and developed. The mechanisms contributing to the material removal and the influence of different parameters on these mechanisms were evaluated. The effects of the WC particle size and volume fraction on the scratch depth and worn volume of the composite were also analyzed at different scratch loads, and the following main conclusions can be drawn from this study:

- The microploughing was the dominant mechanism of material removal of the WC-Ni composite with small WC particle volume fraction at low scratch loads as the substrate tended to pile up on the sides along the scratch length. Also, the material removal mechanism changed from microploughing to microcutting with increasing the particle volume fraction to 30 Vol.% and higher.
- With higher particle volume fraction, the stress was more homogeneously distributed in the case of having smaller WC particles than larger particles, and the stress carrying role of the WC particles in the composite was clearly observed. Also, a large concentration of stress was observed at the interface of the particles and the matrix, which may cause the initiation of material removal. The effect of the particle size and volume fraction on the worn volume varied at different scratch loads due to the relationship that exists between these parameters.
- With an increase in particle size, the impeding penetration of the indenter was more pronounced. This impeding penetration of the indenter helped reduce the worn volume of the composite.

- The worn volume predicted by the ANN model was in agreement with the true worn volume, which shows the capability of the ANN model to predict nonlinear and highly complex wear problems.

5. Acknowledgements

The authors acknowledge funding support from InnoTech Alberta, MITACS, the Natural Science and Engineering Research Council of Canada, the Canada Foundation for Innovation, and the Province of Alberta Ministry of Jobs, Economy, and Innovation. The authors also acknowledge Compute Canada for computing resources.

6. References

[1] A.S.H. Makhlouf, 1 - Current and advanced coating technologies for industrial applications, in: A.S.H. Makhlouf, I.B.T.-N. and U.-T.F. Tiginyanu (Eds.), Woodhead Publ. Ser. Met. Surf. Eng., Woodhead Publishing, 2011: pp. 3–23. https://doi.org/https://doi.org/10.1533/9780857094902.1.3.

[2] L.N. Moskowitz, Application of HVOF thermal spraying to solve corrosion problems in the petroleum industry—an industrial note, J. Therm. Spray Technol. 2 (1993) 21–29. https://doi.org/10.1007/BF02647419.

[3] A.S.H. Makhlouf, High Performance Coatings for Automotive and Aerospace Industries, Nova Science Publishers, Inc, New York, 2010. http://search.ebscohost.com/login.aspx?direct=true&AuthType=ip,url,uid&db=e000xna&AN=346103&site=ehost-live&scope=site.

[4] I.R. Sare, A.G. Constantine, Development of methodologies for the evaluation of wear-

resistant materials for the mineral industry, Wear. 203–204 (1997) 671–678. https://doi.org/https://doi.org/10.1016/S0043-1648(96)07398-X.

[5] V. Hitesh, T. Lalit, S. Harmeet, a Review on Tribo-Corrosion of Coatings in Glass Manufacturing Industry and Performance of Coating Techniques Against High Temperature Corrosion and Wear, I-Manager's J. Mater. Sci. 5 (2017) 38. https://doi.org/10.26634/jms.5.3.13746.

[6] V. Roubicek, H. Raclavska, D. Juchelkova, P. Filip, Wear and environmental aspects of composite materials for automotive braking industry, Wear. 265 (2008) 167–175. https://doi.org/https://doi.org/10.1016/j.wear.2007.09.006.

[7] K. Feng, Y. Chen, P. Deng, Y. Li, H. Zhao, F. Lu, R. Li, J. Huang, Z. Li, Improved high-temperature hardness and wear resistance of Inconel 625 coatings fabricated by laser cladding, J. Mater. Process. Technol. 243 (2017) 82–91. https://doi.org/https://doi.org/10.1016/j.jmatprotec.2016.12.001.

[8] L.A. Franco, A. Sinatora, Material removal factor (fab): A critical assessment of its role in theoretical and practical approaches to abrasive wear of ductile materials, Wear. 382–383 (2017) 51–61. https://doi.org/10.1016/j.wear.2017.04.006.

[9] Y. Li, X. Ge, H. Wang, Y. Hu, F. Ning, W. Cong, C. Ren, Study of material removal mechanisms in grinding of C/SiC composites via single-abrasive scratch tests, Ceram. Int. 45 (2019) 4729–4738. https://doi.org/10.1016/j.ceramint.2018.11.165.

[10] A. Nieto, H. Yang, L. Jiang, J.M. Schoenung, Reinforcement size effects on the abrasive wear of boron carbide reinforced aluminum composites, Wear. 390–391 (2017) 228–235. https://doi.org/https://doi.org/10.1016/j.wear.2017.08.002.

[11] S.A. Alidokht, V.N.V. Munagala, R.R. Chromik, Role of Third Bodies in Friction and Wear of Cold-Sprayed Ti and Ti–TiC Composite Coatings, Tribol. Lett. 65 (2017) 1–15. https://doi.org/10.1007/s11249-017-0899-4.

[12] N.M. Melendez, V. V Narulkar, G.A. Fisher, A.G. McDonald, Effect of reinforcing particles on the wear rate of low-pressure cold-sprayed WC-based MMC coatings, Wear. 306 (2013) 185–195. https://doi.org/https://doi.org/10.1016/j.wear.2013.08.006.

[13] Y. Zhang, Y. Epshteyn, R.R. Chromik, Dry sliding wear behaviour of cold-sprayed Cu-MoS2 and Cu-MoS2-WC composite coatings: The influence of WC, Tribol. Int. 123 (2018) 296–306. https://doi.org/https://doi.org/10.1016/j.triboint.2017.12.015.

[14] Y.T.R. Lee, H. Ashrafizadeh, G. Fisher, A. McDonald, Effect of type of reinforcing particles on the deposition efficiency and wear resistance of low-pressure cold-sprayed metal matrix composite coatings, Surf. Coatings Technol. 324 (2017) 190–200. https://doi.org/10.1016/j.surfcoat.2017.05.057.

[15] A.P. Sannino, H.J. Rack, Dry sliding wear of discontinuously reinforced aluminum composites: review and discussion, Wear. 189 (1995) 1–19. https://doi.org/https://doi.org/10.1016/0043-1648(95)06657-8.

[16] S.A. Alidokht, J. Lengaigne, J.E. Klemberg-Sapieha, S. Yue, R.R. Chromik, Effect of Microstructure and Properties of Ni-WC Composite Coatings on Their Solid Particle Erosion Behavior, J. Mater. Eng. Perform. 28 (2019) 1532–1543. https://doi.org/10.1007/s11665-019-03956-w.

[17] O. Marou Alzouma, M.A. Azman, D.L. Yung, V. Fridrici, P. Kapsa, Influence of different reinforcing particles on the scratch resistance and microstructure of different WC-Ni

composites, Wear. 352–353 (2016) 130–135. https://doi.org/10.1016/j.wear.2016.02.011.

[18] K. Pondicherry, D. Rajaraman, T. Galle, S. Hertelé, D. Fauconnier, P. De Baets, Optimization and Validation of a Load-Controlled Numerical Model for Single Asperity Scratch, Tribol. Lett. 68 (2020) 1–13. https://doi.org/10.1007/s11249-020-1283-3.

[19] C. Trevisiol, A. Jourani, S. Bouvier, Effect of martensite volume fraction and abrasive particles size on friction and wear behaviour of a low alloy steel, Tribol. Int. 113 (2017) 411–425. https://doi.org/10.1016/j.triboint.2016.11.001.

[20] M.X. Shen, F. Dong, Z.X. Zhang, X.K. Meng, X.D. Peng, Effect of abrasive size on friction and wear characteristics of nitrile butadiene rubber (NBR) in two-body abrasion, Tribol. Int. 103 (2016) 1–11. https://doi.org/10.1016/j.triboint.2016.06.025.

[21] T.B. Torgerson, M.D. Harris, S.A. Alidokht, T.W. Scharf, S.M. Aouadi, R.R. Chromik, J.S. Zabinski, A.A. Voevodin, Room and elevated temperature sliding wear behavior of cold sprayed Ni-WC composite coatings, Surf. Coatings Technol. 350 (2018) 136–145. https://doi.org/10.1016/j.surfcoat.2018.05.090.

[22] M. Ben Tkaya, H. Zahouani, S. Mezlini, P. Kapsa, M. Zidi, A. Dogui, The effect of damage in the numerical simulation of a scratch test, Wear. 263 (2007) 1533–1539. https://doi.org/10.1016/j.wear.2007.01.083.

[23] C. Lyphout, G. Bolelli, E. Smazalova, K. Sato, J. Yamada, Š. Houdková, L. Lusvarghi, T. Manfredini, Influence of hardmetal feedstock powder on the sliding wear and impact resistance of High Velocity Air-Fuel (HVAF)sprayed coatings, Wear. 430–431 (2019) 340–354. https://doi.org/10.1016/j.wear.2019.05.016.

[24] K. Holmberg, A. Laukkanen, A. Ghabchi, M. Rombouts, E. Turunen, R. Waudby, T. Suhonen, K. Valtonen, E. Sarlin, Computational modelling based wear resistance analysis of thick composite coatings, Tribol. Int. 72 (2014) 13–30. https://doi.org/10.1016/j.triboint.2013.12.001.

[25] I. Tudela, A.J. Cobley, Y. Zhang, Tribological performance of novel nickel-based composite coatings with lubricant particles, Friction. 7 (2019) 169–180. https://doi.org/10.1007/s40544-018-0211-0.

[26] M. Woldman, E. Van Der Heide, T. Tinga, M.A. Masen, The influence of abrasive body dimensions on single asperity wear, Wear. 301 (2013) 76–81. https://doi.org/10.1016/j.wear.2012.12.009.

[27] J. Li, W. Beres, Scratch Test for Coating/Substrate Systems – A Literature Review, Can. Metall. Q. 46 (2007) 155–173. https://doi.org/10.1179/cmq.2007.46.2.155.

[28] W.M. Gao, L. Wang, J.K. Coffey, F. Daver, Finite element simulation of scratch on polypropylene panels, Mater. Des. 140 (2018) 400–408. https://doi.org/10.1016/j.matdes.2017.12.018.

[29] M.G. Gee, Low load multiple scratch tests of ceramics and hard metals, Wear. 250 (2001) 264–281. https://doi.org/https://doi.org/10.1016/S0043-1648(01)00591-9.

[30] Z. Liu, J. Sun, W. Shen, Study of plowing and friction at the surfaces of plastic deformed metals, Tribol. Int. 35 (2002) 511–522. https://doi.org/https://doi.org/10.1016/S0301-679X(02)00046-4.

[31] T. Futami, M. Ohira, H. Muto, M. Sakai, Contact/scratch-induced surface deformation and

damage of copper–graphite particulate composites, Carbon N. Y. 47 (2009) 2742–2751. https://doi.org/https://doi.org/10.1016/j.carbon.2009.05.034.

[32] D. Verdi, M.A. Garrido, C.J. Múnez, P. Poza, Influence of exposure at high temperature on the local scratch mechanisms in laser cladded Inconel 625-base metal matrix composite coatings, J. Alloys Compd. 733 (2018) 69–81. https://doi.org/10.1016/j.jallcom.2017.10.291.

[33] V. Nemane, S. Chatterjee, Scratch and Sliding Wear Testing of Electroless Ni–B–W Coating, J. Tribol. 142 (2020) 1–9. https://doi.org/10.1115/1.4045165.

[34] K.-H. Zum Gahr, Microstructure and Wear of Materials, in: Elsevier, 1987.

[35] O.A. Zambrano, Y. Aguilar, J. Valdés, S.A. Rodríguez, J.J. Coronado, Effect of normal load on abrasive wear resistance and wear micromechanisms in FeMnAlC alloy and other austenitic steels, Wear. 348–349 (2016) 61–68. https://doi.org/10.1016/j.wear.2015.11.019.

[36] M. Woldman, E. Van Der Heide, T. Tinga, M.A. Masen, A Finite Element Approach to Modeling Abrasive Wear Modes, Tribol. Trans. 60 (2017) 711–718. https://doi.org/10.1080/10402004.2016.1206647.

[37] W. Shi, H. Dong, T. Bell, Tribological behaviour and microscopic wear mechanisms of UHMWPE sliding against thermal oxidation-treated Ti6Al4V, Mater. Sci. Eng. A. 291 (2000) 27–36. https://doi.org/https://doi.org/10.1016/S0921-5093(00)00972-2.

[38] J. Xiaoyu, B. Lauke, T. Schueller, Frictional contact analysis of scratch test for elastic and elastic-plastic thin-coating/substrate materials, Thin Solid Films. 414 (2002) 63–71.

https://doi.org/10.1016/S0040-6090(02)00428-5.

[39] N.X. Randall, The current state-of-the-art in scratch testing of coated systems, Surf. Coatings Technol. 380 (2019) 125092. https://doi.org/https://doi.org/10.1016/j.surfcoat.2019.125092.

[40] M. Varga, S. Leroch, H. Rojacz, M.R. Ripoll, Study of wear mechanisms at high temperature scratch testing, Wear. 388–389 (2017) 112–118. https://doi.org/10.1016/j.wear.2017.04.027.

[41] A. Ul-Hamid, A. Quddus, F.K. Al-Yousef, A.I. Mohammed, H. Saricimen, L.M. Al-Hadhrami, Microstructure and surface mechanical properties of electrodeposited Ni coating on Al 2014 alloy, Surf. Coatings Technol. 205 (2010) 2023–2030. https://doi.org/10.1016/j.surfcoat.2010.08.083.

[42] Z. Rongtao, L. Yanfeng, Z. Xinxi, Z. Jianqiu, Strain-rate sensitivity of scratch hardness and deformation mechanism in nanocrystalline Ni under micro-scratch testing, J. Mater. Sci. 51 (2016) 5889–5900. https://doi.org/10.1007/s10853-016-9890-y.

[43] Z. Rongtao, W. Xian, L. Chaoyong, H. Bintao, L. Yanfeng, Z. Xinxi, Strain-rate dependence of mechanical behavior and deformation mechanisms in bimodal nanostructured Ni under micro-scratch testing, Mech. Mater. 121 (2018) 21–30. https://doi.org/10.1016/j.mechmat.2018.03.005.

[44] S. Mzali, F. Elwasli, A. Mkaddem, S. Mezlini, A micromechanical scratch model to investigate wear mechanisms in UD-GFRP composites, Mech. Ind. 19 (2018). https://doi.org/10.1051/meca/2018011.

[45] J. Hu, D.Y. Li, R. Llewellyn, Computational investigation of microstructural effects on abrasive wear of composite materials, Wear. 259 (2005) 6–17. https://doi.org/10.1016/j.wear.2005.02.017.

[46] J. Hu, D.Y. Li, R. Llewellyn, Synergistic effects of microstructure and abrasion condition on abrasive wear of composites-A modeling study, Wear. 263 (2007) 218–227. https://doi.org/10.1016/j.wear.2007.01.069.

[47] S.P. Jones, R. Jansen, R.L. Fusaro, Preliminary Investigation of Neural Network Techniques to Predict Tribological Properties, Tribol. Trans. 40 (1997) 312–320. https://doi.org/10.1080/10402009708983660.

[48] R. Pramod, G.B. Veeresh Kumar, P.S.S. Gouda, A.T. Mathew, A Study on the Al2O3 reinforced Al7075 Metal Matrix Composites Wear behavior using Artificial Neural Networks, Mater. Today Proc. 5 (2018) 11376–11385. https://doi.org/10.1016/j.matpr.2018.02.105.

[49] D. Satish Kumar, M. Rajmohan, Optimizing Wear Behavior of Epoxy Composites Using Response Surface Methodology and Artificial Neural Networks, Polym. Compos. 40 (2019) 2812–2818. https://doi.org/10.1002/pc.25089.

[50] I.I. Argatov, Y.S. Chai, An artificial neural network supported regression model for wear rate, Tribol. Int. 138 (2019) 211–214. https://doi.org/10.1016/j.triboint.2019.05.040.

[51] A. Shebani, S. Iwnicki, Prediction of wheel and rail wear under different contact conditions using artificial neural networks, Wear. 406–407 (2018) 173–184. https://doi.org/10.1016/j.wear.2018.01.007.

[52] A. Ul-Hamid, H. Dafalla, A. Quddus, H. Saricimen, L.M. Al-Hadhrami, Microstructure and surface mechanical properties of pulse electrodeposited nickel, Appl. Surf. Sci. 257 (2011) 9251–9259. https://doi.org/10.1016/j.apsusc.2011.04.120.

[53] J.L. Bucaille, E. Felder, G. Hochstetter, Mechanical analysis of the scratch test on elastic and perfectly plastic materials with the three-dimensional finite element modeling, Wear. 249 (2001) 422–432. https://doi.org/https://doi.org/10.1016/S0043-1648(01)00538-5.

[54] D. Tabor, The hardness of solids, Rev. Phys. Technol. 1 (1970) 145–179. https://doi.org/10.1088/0034-6683/1/3/i01.

[55] N. Schwarzer, Q.H. Duong, N. Bierwisch, G. Favaro, M. Fuchs, P. Kempe, B. Widrig, J. Ramm, Optimization of the Scratch Test for specific coating designs, Surf. Coatings Technol. 206 (2011) 1327–1335. https://doi.org/10.1016/j.surfcoat.2011.08.051.

[56] S.H. Sajjadi, D. Salimi-Majd, M.J. Ostad Ahmad Ghorabi, Development of a brittle fracture criterion for prediction of crack propagation path under general mixed mode loading, Eng. Fract. Mech. 155 (2016) 36–48. https://doi.org/https://doi.org/10.1016/j.engfracmech.2016.01.015.

[57] A.C. Orifici, I. Herszberg, R.S. Thomson, Review of methodologies for composite material modelling incorporating failure, Compos. Struct. 86 (2008) 194–210. https://doi.org/10.1016/j.compstruct.2008.03.007.

[58] R. Talreja, Multi-scale modeling in damage mechanics of composite materials, J. Mater. Sci. 41 (2006) 6800–6812. https://doi.org/10.1007/s10853-006-0210-9.

[59] G.R. Johnson, W.H. Cook, Fracture characteristics of three metals subjected to various

strains, strain rates, temperatures and pressures, Eng. Fract. Mech. 21 (1985) 31–48. https://doi.org/https://doi.org/10.1016/0013-7944(85)90052-9.

[60] J. Liu, B. Zheng, K. Zhang, B. Yang, X. Yu, Ballistic performance and energy absorption characteristics of thin nickel-based alloy plates at elevated temperatures, Int. J. Impact Eng. 126 (2019) 160–171. https://doi.org/https://doi.org/10.1016/j.ijimpeng.2018.12.012.

[61] J. Wang, X. Hu, K. Yuan, W. Meng, P. Li, Impact resistance prediction of superalloy honeycomb using modified Johnson–Cook constitutive model and fracture criterion, Int. J. Impact Eng. 131 (2019) 66–77. https://doi.org/https://doi.org/10.1016/j.ijimpeng.2019.05.001.

[62] A.S. Khoddami, D. Salimi-Majd, B. Mohammadi, Finite element and experimental investigation of multiple solid particle erosion on Ti-6Al-4V titanium alloy coated by multilayer wear-resistant coating, Surf. Coatings Technol. 372 (2019) 173–189. https://doi.org/10.1016/j.surfcoat.2019.05.042.

[63] B. Mohammadi, A.S. Khoddami, Representative volume element-based simulation of multiple solid particles erosion of a compressor blade considering temperature effect, Proc. Inst. Mech. Eng. Part J J. Eng. Tribol. 234 (2020) 1173–1184. https://doi.org/10.1177/1350650119884825.

[64] M. Shafiq, G. Subhash, Dynamic deformation characteristics of zirconium diboride-silicon carbide under multi-axial confinement, Int. J. Impact Eng. 91 (2016) 158–169. https://doi.org/10.1016/j.ijimpeng.2016.01.009.

[65] T.J. Holmquist, G.R. Johnson, Response of boron carbide subjected to high-velocity impact, Int. J. Impact Eng. 35 (2008) 742–752.

https://doi.org/10.1016/j.ijimpeng.2007.08.003.

[66] T.J. Holmquist, D.W. Templeton, K.D. Bishnoi, Constitutive modeling of aluminum nitride for large strain, high-strain rate, and high-pressure applications, Int. J. Impact Eng. 25 (2001) 211–231. https://doi.org/10.1016/S0734-743X(00)00046-4.

[67] T.J. Holmquist, G.R. Johnson, Response of silicon carbide to high velocity impact, J. Appl. Phys. 91 (2002) 5858–5866. https://doi.org/10.1063/1.1468903.

[68] G.R. Johnson, T.J. Holmquist, An improved computational constitutive model for brittle materials, in: AIP Conf. Proc., AIP, 1994: pp. 981–984. https://doi.org/10.1063/1.46199.

[69] Y.M. Xia, B. Guo, G.Q. Cong, X.H. Zhang, G.Y. Zeng, Numerical simulation of rock fragmentation induced by a single TBM disc cutter close to a side free surface, Int. J. Rock Mech. Min. Sci. 91 (2017) 40–48. https://doi.org/https://doi.org/10.1016/j.ijrmms.2016.11.004.

[70] J.F. Moxnes, J.A. Teland, S. Skriudalen, S.M. Bergsrud, L. Sundem-Eriksen, H. Fykse, Development of material models for semi-brittle materials like tungsten carbide, 2010.

[71] R. Ghelichi, S. Bagherifard, M. Guagliano, M. Verani, Numerical simulation of cold spray coating, Surf. Coatings Technol. 205 (2011) 5294–5301. https://doi.org/10.1016/j.surfcoat.2011.05.038.

[72] T.J. Holmquist, G.R. Johnson, W.A. Gooch, Modeling the 14.5 mm BS41 projectile for ballistic impact computations, 40 (2014) 73–86. https://doi.org/10.2495/978-1-84564-879-4/008.

[73] H.K. Ghritlahre, R.K. Prasad, Application of ANN technique to predict the performance

of solar collector systems - A review, Renew. Sustain. Energy Rev. 84 (2018) 75–88. https://doi.org/https://doi.org/10.1016/j.rser.2018.01.001.

[74] A.S. Ahmad, M.Y. Hassan, M.P. Abdullah, H.A. Rahman, F. Hussin, H. Abdullah, R. Saidur, A review on applications of ANN and SVM for building electrical energy consumption forecasting, Renew. Sustain. Energy Rev. 33 (2014) 102–109. https://doi.org/https://doi.org/10.1016/j.rser.2014.01.069.

[75] H. El Kadi, Modeling the mechanical behavior of fiber-reinforced polymeric composite materials using artificial neural networks—A review, Compos. Struct. 73 (2006) 1–23. https://doi.org/https://doi.org/10.1016/j.compstruct.2005.01.020.

[76] I. Mukherjee, P.K. Ray, A review of optimization techniques in metal cutting processes, Comput. Ind. Eng. 50 (2006) 15–34. https://doi.org/10.1016/j.cie.2005.10.001.

[77] I. Argatov, Artificial Neural Networks (ANNs) as a Novel Modeling Technique in Tribology, Front. Mech. Eng. 5 (2019) 1–9. https://doi.org/10.3389/fmech.2019.00030.

[78] M. Zakeri, A. Bahrami, S.H. Mousavi Anijdan, Using genetic algorithm in heat treatment optimization of 17-4PH stainless steel, Mater. Des. 28 (2007) 2034–2039. https://doi.org/https://doi.org/10.1016/j.matdes.2006.06.006.

[79] D.T. Oyekunle, T.I. Oguntade, C.S. Ita, T. Ojo, O.D. Orodu, Corrosion inhibition of mild steel using binary mixture of sesame and castor oil in brine solution, Mater. Today Commun. 21 (2019) 100691. https://doi.org/https://doi.org/10.1016/j.mtcomm.2019.100691.

[80] M.A.R. Mojena, A.S. Roca, R.S. Zamora, M.S. Orozco, H.C. Fals, C.R.C. Lima, Neural

network analysis for erosive wear of hard coatings deposited by thermal spray: Influence of microstructure and mechanical properties, Wear. 376–377 (2017) 557–565. https://doi.org/https://doi.org/10.1016/j.wear.2016.12.035.

[81] J. Adnan, N.G.N. Daud, M.T. Ishak, Z.I. Rizman, M.I.A. Rahman, Tansig activation function (of MLP network) for cardiac abnormality detection, AIP Conf. Proc. 1930 (2018). https://doi.org/10.1063/1.5022900.

[82] F.R. Bin Hashim, J.J. Soraghan, L. Petropoulakis, Multi-classify Hybrid Multilayered Perceptron (HMLP) Network for Pattern Recognition Applications, in: L. Iliadis, I. Maglogiannis, H. Papadopoulos (Eds.), Artif. Intell. Appl. Innov., Springer Berlin Heidelberg, Berlin, Heidelberg, 2012: pp. 19–27.

[83] M.H. Beale, M.T. Hagan, Neural Network Toolbox™ User's Guide, The MathWorks; Inc. 3 Apple Hill Drive Natick; MA 01760-2098, (2015) 410. https://doi.org/10.1016/j.neunet.2005.10.002.

[84] K. Swingler, Applying Neural Netwrok. A Practical Guide, in: Morgan Kaufman Publishers Inc., San Francisco, California, 2001: pp. 3–75.

[85] S. Haykin, Neural Networks: A Comprehensive Foundation, 2nd ed., Pearson, New Jersey, 1999.

[86] W.H. Delashmit, L.M. Missiles, Recent Developments in Multilayer Perceptron Neural Networks, Proc. 7th Annu. Memphis Area Eng. Sci. Conf. (2005) 1–15. http://citeseerx.ist.psu.edu/viewdoc/summary?doi=10.1.1.318.4243.

[87] J.K. Xiao, L. Zhang, K.C. Zhou, X.P. Wang, Microscratch behavior of copper-graphite

composites, Tribol. Int. 57 (2013) 38–45. https://doi.org/10.1016/j.triboint.2012.07.004.

[88] M. Ben Tkaya, S. Mezlini, M. El Mansori, H. Zahouani, On some tribological effects of graphite nodules in wear mechanism of SG cast iron: Finite element and experimental analysis, Wear. 267 (2009) 535–539. https://doi.org/10.1016/j.wear.2009.01.058.

[89] H. Cao, W. Ma, H. Chen, Q. Wang, Y. Wang, Core-rim microstructure and properties of WC/Ni composites, Int. J. Refract. Met. Hard Mater. 78 (2019) 170–177. https://doi.org/10.1016/j.ijrmhm.2018.09.007.

[90] R.G. Bayer, R.A. Schumacher, On the significance of surface fatigue in sliding wear, Wear. 12 (1968) 173–183. https://doi.org/https://doi.org/10.1016/0043-1648(68)90524-3.

[91] K. Jia, T.E. Fischer, B. Gallois, Microstructure, hardness and toughness of nanostructured and conventional WC-Co composites, Nanostructured Mater. 10 (1998) 875–891. https://doi.org/https://doi.org/10.1016/S0965-9773(98)00123-8.

[92] Z. Wang, P. Gu, H. Zhang, Z. Zhang, X. Wu, Finite element modeling of the indentation and scratch response of epoxy/silica nanocomposites, Mech. Adv. Mater. Struct. 21 (2014) 802–809. https://doi.org/10.1080/15376494.2012.707752.

[93] S.A. Alidokht, P. Manimunda, P. Vo, S. Yue, R.R. Chromik, Cold spray deposition of a Ni-WC composite coating and its dry sliding wear behavior, Surf. Coatings Technol. 308 (2016) 424–434. https://doi.org/10.1016/j.surfcoat.2016.09.089.

[94] Z.F. Zhang, L.C. Zhang, Y.W. Mai, Particle effects on friction and wear of aluminium matrix composites, J. Mater. Sci. 30 (1995) 5999–6004. https://doi.org/10.1007/BF01151519.

[95] S.P. Dwivedi, S. Sharma, R.K. Mishra, Comparison of Microstructure and Mechanical Properties of A356/SiC Metal Matrix Composites Produced by Two Different Melting Routes, Int. J. Manuf. Eng. 2014 (2014) 1–13. https://doi.org/10.1155/2014/747865.

[96] D. Kong, Y. Chen, N. Li, Gaussian process regression for tool wear prediction, Mech. Syst. Signal Process. 104 (2018) 556–574. https://doi.org/https://doi.org/10.1016/j.ymssp.2017.11.021.

[97] O. Altay, T. Gurgenc, M. Ulas, C. Özel, Prediction of wear loss quantities of ferro-alloy coating using different machine learning algorithms, 8 (2020) 107–114.

[98] P.R. Pati, Prediction and wear performance of red brick dust filled glass–epoxy composites using neural networks, Int. J. Plast. Technol. 23 (2019) 253–260. https://doi.org/10.1007/s12588-019-09257-0.

[99] P.K. Padhi, A. Satapathy, Analysis of Sliding Wear Characteristics of BFS Filled Composites Using an Experimental Design Approach Integrated with ANN, Tribol. Trans. 56 (2013) 789–796. https://doi.org/10.1080/10402004.2013.798448.

Declaration of interests

☒ The authors declare that they have no known competing financial interests or personal relationships that could have appeared to influence the work reported in this paper.

☐The authors declare the following financial interests/personal relationships which may be considered as potential competing interests:

Author Agreement Statement

We the undersigned declare that this manuscript is original, has not been published before and is not currently being considered for publication elsewhere.

We confirm that the manuscript has been read and approved by all named authors and that there are no other persons who satisfied the criteria for authorship but are not listed. We further confirm that the order of authors listed in the manuscript has been approved by all of us.

We understand that the Corresponding Author is the sole contact for the Editorial process. He/she is responsible for communicating with the other authors about progress, submissions of revisions and final approval of proofs

Signed by corresponding author on behalf of all authors.

Corresponding author signature Date: October 23, 2020